Mon. Not. R. Astron. Soc. **000**, 1–20 (2005) Printed 5 February 2008 (MN LATEX style file v2.2)

Southern GEMS Groups I: Dynamical Properties

Sarah Brough[1⋆], Duncan A. Forbes[1], Virginia A. Kilborn[1,2], Warrick Couch[3]
[1] *Centre for Astrophysics and Supercomputing, Swinburne University of Technology, Hawthorn, VIC 3122, Australia*
[2] *Australia Telescope National Facility, CSIRO, P.O. Box 76, Epping, NSW 1710, Australia*
[3] *School of Physics, The University of New South Wales, Sydney, NSW 2052, Australia*

Accepted... Received...; in original form 2005

ABSTRACT

Here we present an investigation of the properties of 16 nearby galaxy groups and their constituent galaxies. The groups are selected from the Group Evolution Multiwavelength Study (GEMS) and all have X-ray as well as wide-field neutral hydrogen (HI) observations. Group membership is determined using a friends-of-friends algorithm on the positions and velocities from the 6-degree Field Galaxy Survey (6dFGS) and NASA/IPAC Extra-galactic Database (NED). For each group we derive their physical properties using this membership, including: velocity dispersions (σ_v), virial masses (M_V), total K-band luminosities ($L_K(Tot)$) and early-type fractions (f_{early}) and present these data for the individual groups. We find that the GEMS X-ray luminosity is proportional to the group velocity dispersions and virial masses: $L_X(r_{500}) \propto \sigma_v^{3.11\pm0.59}$ and $L_X(r_{500}) \propto M_V^{1.13\pm0.27}$, consistent with the predictions of self-similarity between group and clusters. We also find that $M_V \propto L_K(Tot)^{2.0\pm0.9}$, i.e. mass grows faster than light and that the fraction of early-type galaxies in the groups is correlated with the group X-ray luminosities and velocity dispersions. We examine the brightest group galaxies (BGGs), finding that, while the luminosity of the BGG correlates with its total group luminosity, the fraction of group luminosity contained in the BGG decreases with increasing total group luminosity. This suggests that BGGs grow by mergers at early times in group evolution while the group continues to grow by accreting infalling galaxies. We form a composite galaxy group in order to examine the properties of the constituent galaxies and compare their properties with those of field galaxies. There are clear radial trends, with group galaxies becoming fainter, bluer and morphologically later types with increasing radius from the group centre, reaching field levels at radii $> r_{500} (> 0.7 r_{200})$. We divide the composite group by group X-ray luminosity and find that galaxies in high X-ray luminosity groups ($\log_{10} L_X(r_{500}) \geqslant 41.7$ erg s^{-1}) are redder with a higher giant-to-dwarf ratio and are more likely to be early-type galaxies than are those galaxies in low X-ray luminosity groups. We conclude that harrassment and ram pressure stripping processes are unlikely to cause these differences. The differences are more likely to be due to galaxy-galaxy mergers and possibly some further mechanism such as strangulation. If mergers are the dominant mechanism then the properties of galaxies in the higher X-ray luminosity groups are a result of mergers at earlier epochs in smaller mass groups that have since merged to become the structures we observe today, while lower X-ray luminosity groups are still undergoing mergers today.

Key words: Surveys – galaxies: evolution – galaxies: formation – galaxies: fundamental parameters

1 INTRODUCTION

It has been known for many years that galaxies in denser environments are in general redder and brighter (e.g. Faber 1973; Oemler 1974; Visvanathan & Sandage 1977; Butcher & Oemler 1984) and are more likely to be early-type galaxies showing little signs of recent star formation than those in less dense environments (e.g. Dressler 1980). Recent galaxy surveys have shown that the density at which the observed properties of galaxies change from those of the field to those of more dense environments is $\sim 2-3$ virial radii in clusters (e.g. Lewis et al. 2002), and that the galaxy

⋆ E-mail: sbrough@astro.swin.edu.au

density at these radii is equivalent to that of the density in poor galaxy groups (e.g. Gómez et al. 2003).

The proposed mechanisms to transform the properties of galaxies are, therefore, environmentally dependent. The processes acting on galaxies in the group environment are different to those acting in the cluster environment: Ram pressure stripping (e.g. Gunn & Gott 1972; Quilis et al. 2000) and harassment (Moore et al. 1996) are more likely to be dominant in the dense, but rare, environments of clusters. However, mergers and strangulation are more likely in the group environment, where the velocity dispersion of the group is similar to that of its constituent galaxies (Barnes 1985; Zabludoff & Mulchaey 1998; Hashimoto & Oemler 2000) and galaxies are predicted to be falling into a dense environment from the field for the first time.

Due to the small numbers of galaxies in an individual group and their wide spatial distribution compared to a cluster, groups are a relatively understudied environment. However, galaxy groups are significantly more abundant than galaxy clusters and most galaxies in the local Universe are found in group, rather than cluster, environments (e.g. Eke et al. 2004a). Considering the importance of this environment it is vital that this is remedied. It is therefore important to study the properties of groups and their constituent galaxies. Multi-wavelength observations are vital to determine which evolutionary processes are dominant in this environment. While optical spectra and near-infrared imaging provide dynamical information on the groups and morphologies of individual galaxies, X-ray observations provide information on the mass and dynamical state of the group and neutral hydrogen (HI) observations show us regions of potential star formation, and provide direct evidence of interactions through tidal material.

2 GROUP SAMPLE

The Group Evolution Multiwavelength Study (GEMS; Osmond & Ponman 2004; Forbes et al. 2006) is an ongoing study of 60 groups with a range of optical and X-ray properties. The group selection is described in detail in Osmond & Ponman (2004). In addition to calculating the X-ray luminosity of each group, which is proportional to the gas density in the potential and hence mass, Osmond & Ponman (2004) also determine whether the groups have intra-group X-ray emission, X-ray emission solely from a galaxy halo or, if the X-ray flux was $< 3\sigma$ above the background level, defined the group as undetected. Wide-field neutral hydrogen (HI) observations of 16 GEMS groups in the Southern hemisphere were made with the Parkes radiotelescope (Kilborn et al. in preparation).

Osmond & Ponman (2004) defined the optical properties of the GEMS groups within a radius corresponding to an overdensity of 500 times the critical density – r_{500}. Galaxies were obtained from the NASA/IPAC Extragalactic Database (NED) within r_{500}. The optical data were used to calculate the mean velocity, $\bar{v}$, and velocity dispersion, σ_v, of the groups and the updated values were used to refine the search criteria. The selection and recalculation were repeated until the values of $\bar{v}$ and σ_v were stable. The dynamical properties of the groups were then calculated for the galaxies within r_{500}. In some cases there was only 1 galaxy member within r_{500} preventing a measurement of dynamical properties.

Here we re-analyse the optical properties of the 16 groups with HI observations using a 'friends-of-friends' percolation algorithm (FOF; Huchra & Geller 1982) to determine group membership. We then compare the groups' optical properties with their X-ray properties. The HI properties of these groups will be analysed in Kilborn et al. (in preparation).

Unlike Osmond & Ponman (2004) where galaxies are defined as group members if they are within a specific radius and velocity range of each centroid, FOF determines which galaxies are associated with one another in position and velocity space and does not rely on any *a priori* assumption about the geometrical shape of groups. We use the 6-degree Field Galaxy Survey (6dFGS; Jones et al. 2004) to obtain galaxy velocities for this sample of 16 groups and emphasize that every galaxy in our analysis has measured recession velocities, freeing our statistical analyses from projection effects and providing a significant advantage over some previous studies. We examine the Two-micron All Sky Survey (2MASS; Jarrett et al. 2000) near-infrared magnitudes and colours of the constituent galaxies. These magnitudes provide an advantage over the B-band magnitudes used by Osmond & Ponman (2004) as the light from the near-infrared is more closely related to galaxy mass. We also stack galaxies in the groups to create a composite group with galaxy numbers comparable to those in a cluster, in order to better understand the properties of the groups.

The dynamical properties of two of these groups, NGC 1332 and NGC 1407 were discussed in Brough et al. (2006). Those results are updated and the remaining 14 groups presented and discussed in this paper. The group properties and X-ray attributes of the groups derived by Osmond & Ponman (2004) are given in Table 1 – G indicates groups with intra-group X-ray emission (i.e. X-ray extent > 60 kpc), H indicates groups with only galaxy-halo emission (i.e. emission $\leqslant 60$ kpc) and U indicates that the X-ray flux from that region was $< 3\sigma$ above the background level and the group is therefore undetected in X-rays. Eight of the groups in this sample show X-ray emission, 6 show solely galaxy-halo emission and 2 are undetected in X-rays. The NGC 3783, NGC 7144 and NGC 7714 groups had less than 4 members within r_{500} in Osmond & Ponman (2004) and do not appear in their final statistical analysis.

The outline of the paper is as follows: We introduce our data in Section 3 and in Section 4 we discuss our method of determining group membership using these data. The dynamical properties of the groups based on that membership are presented in Section 5 and the properties of the individual groups are discussed in Section 6. The relations between the X-ray and dynamical properties of the groups are presented in Section 8 and the properties of the brightest group galaxies in Section 9. Our analysis of the galaxies in each group stacked to create a composite group is presented in Section 10 and we draw our conclusions in Section 11. As in previous GEMS papers we assume $H_0 = 70$ km s^{-1} Mpc^{-1}.

Table 1. Group properties defined by Osmond & Ponman (2004) using the distances calculated in that paper. Dashes indicate where information is not available.

Group Name	N	$\bar{v}$ (km s^{-1})	σ_v (km s^{-1})	r_{500} (Mpc)	$\log_{10}L_X$ (r_{500}) (erg s^{-1})	T_X (keV)	X-ray emission
NGC 524	10	2470±55	175±42	0.45	41.33±0.05	0.65±0.07	H
NGC 720	4	1640±136	273±122	0.40	41.43±0.02	0.52±0.03	G
NGC 1052	5	1366±41	91±35	0.36	40.53±0.15	0.41±0.15	H
NGC 1332	10	1489±59	186±45	0.42	40.93±0.02	0.56±0.03	H
NGC 1407	20	1682±71	319±52	0.57	41.92±0.02	1.02±0.04	G
NGC 1566	9	1402±61	184±47	0.47	40.85±0.05	0.70±0.11	H
NGC 1808	4	1071±52	104±47	0.32	< 40.59	–	U
NGC 3557	14	2858±80	300±60	0.27	42.11±0.04	0.24±0.02	G
NGC 3783	1	2917	–	0.25	40.94±0.11	–	G
NGC 3923	8	1764±85	239±66	0.40	41.07±0.02	0.52±0.03	H
NGC 4636	9	936±95	284±73	0.51	41.71±0.02	0.84±0.02	G
NGC 5044	18	2518±100	426±74	0.62	43.09±0.01	1.21±0.02	G
NGC 7144	2	1912 ±29	41±41	0.38	40.71±0.13	–	H
HCG 90	15	2559±34	131±25	0.38	41.79±0.05	0.46±0.07	G
IC 1459	8	1835±79	223±62	0.35	41.46±0.04	0.39±0.04	G
NGC 7714	2	2784±20	28±28	0.22	< 40.48	–	U

The columns indicate (1) Group name, (2) Number of group members within r_{500}, (3) Mean velocity of group and 1σ error, (4) Velocity dispersion and 1σ error, (5) r_{500} radius, (6) *ROSAT* PSPC X-ray luminosity extrapolated to the r_{500} radius and 1σ error, (7) *ROSAT* PSPC X-ray temperature and 1σ error, (8) indicates whether the X-ray emission is from intra-group gas (G), a galaxy halo (H) or is $< 3\sigma$ background (U).

3 DATA

The 6dFGS is a wide-area (the entire southern sky with $|b| > 10^o$), primarily K_s-band selected galaxy redshift survey. The catalogue provides positions, recession velocities, and spectra for the galaxies, along with total K_s-band magnitudes adapted from the 2MASS catalogue (Jones et al. 2004).

The second data release of the 6dFGS (DR2; Jones et al. 2005) contains 71,627 unique galaxies. We obtained data for 13 of the 16 groups from this catalogue for a square of $\sim 5.5^\circ \times 5.5^\circ$ around the position of each group defined by Osmond & Ponman (2004). This area is chosen to match the HI observations. However, we extended the search regions around the NGC 1332, NGC 1407 and NGC 4636 groups. NGC 1332 and NGC 1407 occupy the same region of sky and a circle of radius 15° was examined around these galaxies in Brough et al. (2006). NGC 4636 lies south of the Virgo cluster centre and it was necessary to extend the study to $15^\circ \times 15^\circ$ to determine a boundary with the Virgo cluster. In all the datasets we limited the data to recession velocities $500 < v < 5000$ km s^{-1}, with the exception of NGC 1332 and NGC 1407 which are limited to $v < 2500$km s^{-1}. The lower limit was chosen to avoid Galactic confusion. The search regions and numbers of galaxies found are summarised in Table 2. The 6dFGS database also provides 2MASS K_s-band magnitudes where available. We have used the 2MASS K_s magnitudes within the 20th magnitude isophote (henceforth denoted as K). As 2MASS is > 99 per cent complete to $m_K \sim 13.1$ (Jarrett et al. 2000) we assume that those galaxies without K magnitudes are fainter than the 2MASS magnitude limit.

3.1 NED

We have 3 groups in the Northern sky for which 6dFGS data is not available (NGC 524, NGC 4636 and NGC 7714). The 6dFGS is also not yet complete. We therefore supplemented the 6dFGS data with sources with known recession velocities from the NASA/IPAC Extragalactic Database (NED) in the same position and velocity range. This added an extra 1220 unique galaxies, also detailed in Table 2. The total number of galaxies from NED and 6dFGS is 1735.

NED is a heterogeneous data resource. We illustrated in Brough et al. (2006) that using NED our sample is complete in photometry and velocity to a minimum of $K \leqslant 11$ mag, and that including data fainter than this has little effect, within the errors, on the results we obtain.

3.2 HI

Kilborn et al. (in preparation) details new galaxies found in the Parkes HI maps of these 16 groups and also the velocities found for previously catalogued galaxies without known velocities. We use these new data in our dynamical analysis and the numbers for each region are summarised in Table 2. These galaxies are all fainter than the 2MASS apparent-magnitude limit ($m_K \sim 13.1$; Jarrett et al. 2000).

3.3 Magnitudes

To avoid the effects of peculiar velocities which are significant at recession velocities less than 2000 km s^{-1} (Marinoni et al. 1998) we use independent distances in order to calculate the absolute magnitudes. The distances are primarily from the distance moduli (DM) from surface brightness fluctuation studies by Tonry et al. (2001), corrected following the work of Jensen et al. (2003), indicated by 'TJ' in

Table 2. The distance modulus to the NGC 1332 and NGC 1407 groups is calculated from the NGC 1407 galaxy globular cluster luminosity function of Forbes et al. (2006), denoted by 'F' in Table 2. Distances for the remaining groups were calculated by Osmond & Ponman (2004) from their mean group velocities after correcting for the infall into Virgo and the Great Attractor, denoted 'O' in Table 2. Absolute magnitudes are calculated as $M = m - DM - A$. Galactic Extinction (A) is calculated using the extinction maps of Schlegel et al. (1998) and is of the order $A_K \sim 0.01$ mag and $A_B \sim 0.09$ mag.

4 GROUP MEMBERSHIP

In order to study the dynamics of these groups it is important to determine which galaxies are associated with each other in each field. We used the FOF percolation algorithm which finds group structures in galaxy data based on positional and velocity information and does not rely on any *a priori* assumption about the geometrical shape of groups. As we are examining a small range in recession velocities we do not adopt the method used by Huchra & Geller (1982) to compensate for the sampling of the galaxy luminosity function as a function of the distance of the group.

Owing to the similarity in sampling between the 2dFGRS and 6dFGS at these recession velocities we follow the prescriptions of the 2dFGRS Percolation-Inferred Galaxy Group (2PIGG; Eke et al. 2004a) catalogue to determine the most appropriate value of limiting density contrast, $\delta\rho/\rho$,

$$\frac{\delta\rho}{\rho} = \frac{3}{4}\pi D_0^3 \left[\int_{-\infty}^{M_{lim}} \phi(M) dM\right]^{-1} - 1. \quad (1)$$

The number density contour surrounding each group represents a fixed number density enhancement relative to the mean number density. We assume the differential galaxy luminosity function defined by Kochanek et al. (2001), which Ramella et al. (2004) determine to be a good approximation for the K-band groups luminosity function ($M_\star = -22.6$, $\alpha = -1.09$ and $\phi_\star = 0.004$ for $H_0 = 70$ km s^{-1} Mpc^{-1}). The 2PIGG limiting density contrast $\delta\rho/\rho = 150$ then gives $D_0 = 0.29$ Mpc. We also follow 2PIGG to calculate our velocity limit, V_0. The peculiar motion of galaxies moving in a gravitational potential lengthens the group along the line-of-sight in velocity space – giving the 'Finger of God' effect. If we assume that the projected spatial (D_0) and the line-of-sight dimensions of a group in velocity space (V_0) are in proportion, Eke et al. (2004a) show that a ratio of 12 for V_0 relative to D_0 is the most appropriate for a linking volume, giving $V_0 = 347$ km s^{-1} here.

The FOF algorithm was run over the whole sample of galaxies in each region. We remove all groups with $N \leqslant 3$ galaxies as these have been shown by many surveys to be significantly more likely to be false positives found by the FOF algorithm (e.g. Ramella et al. 1995; Nolthenius et al. 1997; Diaferio et al. 1999).

Groups corresponding to the positions and velocities presented in Osmond & Ponman (2004) were found in 15 out of the 16 groups. In contrast, no group with > 3 members was found in the NGC 7144 field. This group was initially determined to consist of three galaxies (NGC 7155, NGC 7144 and NGC 7145) by Huchra & Geller (1982). Tully (1987) used a hierarchical group finding technique and found a group consisting of the same 3 galaxies in his Nearby Galaxies Catalogue. Maia et al. (1989) analysed the Southern Sky Redshift Survey (SSRS, da Costa et al. 1988) with a FOF analysis and added a new group member (NGC 7151). Garcia (1993) examined the LEDA database using both FOF and hierarchical group-finding techniques and added a further new group member (ESO 236-G035). There is no obvious group system present in the optical data, suggesting that previous group finders were tuned to find looser structures. There is no group X-ray emission in this region, only emission associated with the NGC 7144 galaxy and Osmond & Ponman (2004) only found two galaxies associated with this group. Thus, contrary to earlier claims, we do not find evidence for a group and do not discuss this group further, leaving a sample of 15 groups.

We compared the groups defined by taking three different density contrasts: $\delta\rho/\rho = 100$ (i.e. less dense than the 2PIGG catalogue), $\delta\rho/\rho = 150$ (the 2PIGG value) and $\delta\rho/\rho = 200$ (i.e. more dense). We find in 4 groups (NGC 1566, NGC 1808, NGC 3557 and NGC 3783) that there is no change in group membership and therefore none in mean velocity or velocity dispersion. For all 15 groups we find the mean difference in group members to be $\langle\Delta N(150-200)\rangle = 2.6 \pm 0.9$ and $\langle\Delta N(150-100)\rangle = -6.8 \pm 3.3$ i.e. on average, there are less galaxies if the density contrast is increased and more galaxies if it is lowered, as expected. Comparing the velocity dispersions calculated for the different memberships we can examine the effect of the choice of density contrast on the calculated dynamical parameters: $\langle\Delta\sigma_v(150-200)\rangle = 25 \pm 17$ km s^{-1} and $\langle\Delta\sigma_v(150-100)\rangle = 3 \pm 7$ km s^{-1}. These differences are smaller than the errors on the calculated velocity dispersions and, within the error on the mean difference, consistent with no difference. We therefore conclude that the group properties defined by FOF are robust to the choice of density contrast and present results using the 2PIGG $\delta\rho/\rho = 150$ in Table 3. The galaxies determined to be group members are listed in Appendix A. The spatial distribution and velocity-distance diagrams for these groups are illustrated in Appendix B.

The velocity dispersions derived using the membership determined by FOF are compared in Figure 1 with those derived by Osmond & Ponman (2004). As Osmond & Ponman (2004) only determined one member within r_{500} for the NGC 3783 group, no velocity dispersion was measured. As a result, this group is substantially offset in Figure 1. The mean difference between the two samples is $\langle\Delta\sigma_v\rangle = -8 \pm 17$ km s^{-1}, i.e. consistent with no difference.

5 DYNAMICAL PROPERTIES OF GROUPS

The dynamical properties are calculated in the same way as introduced in Brough et al. (2006): For each group defined by the FOF algorithm the luminosity-weighted centroid and mean recession velocity were calculated. These and the dynamical parameters calculated using the FOF group members are summarised in Table 3.

The velocity dispersion, σ_v, was calculated using the gapper algorithm (Beers et al. 1990):

Table 2. Search regions, distances, and sources of galaxy data for each group.

Group	Min RA (J2000)	Max RA (J2000)	Min Dec (J2000)	Max Dec (J2000)	D (Mpc)	6dFGS (sources)	HI (sources)	NED (sources)	Total
NGC 524	1:14	1:34	06:30	12:00	22.3 (TJ)	0	0	33	33
NGC 720	1:40	2:03	-16:30	-11:00	25.7 (TJ)	6	3	10	19
NGC 1052	2:28	2:52	-11:15	-05:45	18.0 (TJ)	30	0	42	72
NGC 1332	2:16	4:40	-6:00	-36:00	20.9 (F)	158	0	499	657
NGC 1407	2:16	4:40	-6:00	-36:00	20.9 (F)	158	0	499	657
NGC 1566	3:54	4:36	-58:30	-52:30	21.0 (O)	9	2	18	29
NGC 1808	4:55	5:23	-40:30	-35:00	17.0 (O)	17	0	5	22
NGC 3557	10:55	11:24	-40:45	-34:30	42.5 (TJ)	36	3	17	56
NGC 3783	11:10	12:05	-43:00	-33:00	36.0 (TJ)	81	3	27	111
NGC 3923	11:25	12:15	-34:00	-23:00	21.3 (O)	92	2	29	123
NGC 4636	12:24	13:05	-02:00	08:00	13.6 (TJ)	0	1	352	353
NGC 5044	13:02	13:27	-19:15	-13:30	29.0 (TJ)	25	6	56	87
NGC 7144	21:36	22:12	-51:30	-46:00	22.8 (TJ)	1	3	15	19
HCG 90	21:48	22:15	-35:30	-30:30	36.0 (O)	39	0	66	105
IC 1459	22:42	23:12	-40:00	-33:30	27.2 (TJ)	21	0	26	47
NGC 7714	23:25	23:47	-01:30	04:30	39.0 (O)	0	1	25	26

The columns indicate (1) Group name; (2), (3), (4) and (5) outline the Right Ascension and Declination range over which the 6dFGS and NED searches were made; (6) distance [from Tonry et al. (2001) corrected following Jensen et al. (2003; TJ), Forbes et al. (2005; F) or Osmond & Ponman (2004; O)]; (7) Number of sources in the group region from the 6dFGS catalogue; (8) Number of sources in the group region from the HI survey of Kilborn et al. (in preparation); (9) Number of sources in the group region from NED; (10) Total number of sources in each region.

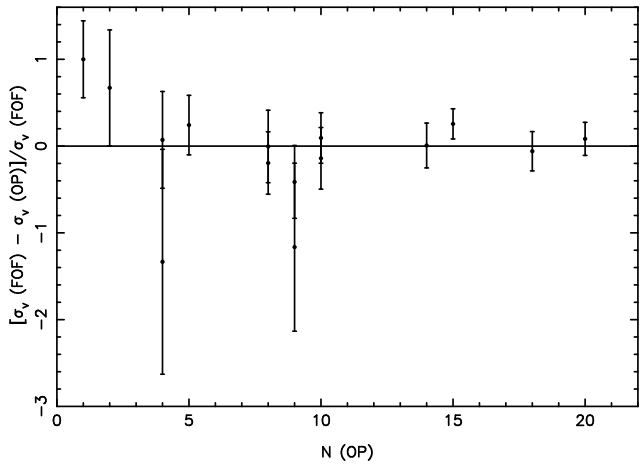

Figure 1. Comparing the velocity dispersions calculated by Osmond & Ponman (2004), $\sigma_v(OP)$, and those calculated using the FOF membership, $\sigma_v(FOF)$ with the number of members assigned by Osmond & Ponman, N (OP). Error bars indicate the combined 1σ errors on the velocity dispersions.

$$\sigma_v = c\sqrt{\frac{\pi}{[n(n-1)]}}\sum_{i=1}^{n-1} w_i g_i, \tag{2}$$

where $w_i = i(n-i)$ and $g_i = z(i+1) - z(i)$. This method is insensitive to outliers, giving a robust estimate of σ_v for small groups. The corresponding errors are estimated using the jackknife algorithm.

The crossing time is calculated as a function of the Hubble time (H_0^{-1}) following Huchra & Geller (1982), as:

$$t_c = \frac{3\ r_H}{5^{3/2}\sigma_v}, \tag{3}$$

where the harmonic radius, r_H, is independent of the velocity dispersion and is given below.

$$r_H = \pi\ D\ sin\ \left[\frac{n(n-1)}{2\sum_i\sum_{j>i}\theta_{ij}^{-1}}\right], \tag{4}$$

where D is the distance to the group given in Table 2, n is the number of members of each group, and θ_{ij}^{-1} is the angular separation of group members. The errors on r_H are estimated using the jackknife method and the errors on t_c are calulcated using standard error propagation analysis. Nolthenius & White (1987) indicate that a crossing time $> 0.09\ H_0^{-1}$ suggests that a group has not yet had time to virialize.

The virial mass M_V was calculated using the virial mass mass estimator of Heisler et al. (1985).

$$M_V = \frac{3\ \pi\ N}{2\ G}\frac{\sum_i V_i^2}{\sum_{i<j} 1/R_{gc,ij}}, \tag{5}$$

where V_i is the observed radial component of the velocity of the galaxy i with respect to the systemic group velocity and $R_{gc,ij}$ is its projected, group-centric, separation from other group members. This assumes that the group is virialised. If the group is not virialised then the calculated virial mass will be an underestimate of the true value. However, Mamon (1993) show that this is not a large effect. We estimate the rms error on the virial mass using the jackknife method.

The radius corresponding to an overdensity of 500 times the critical density – r_{500}, provides a measure of the size of a group. This radius is equivalent to $\sim 1.5 r_{200}$, the virial radius, but is a more robust measure of size than r_{200} at the low densities of groups. We calculate r_{500} as a function of the velocity dispersion calculated above, following Osmond & Ponman (2004) as,

Table 3. Landscape table goes here

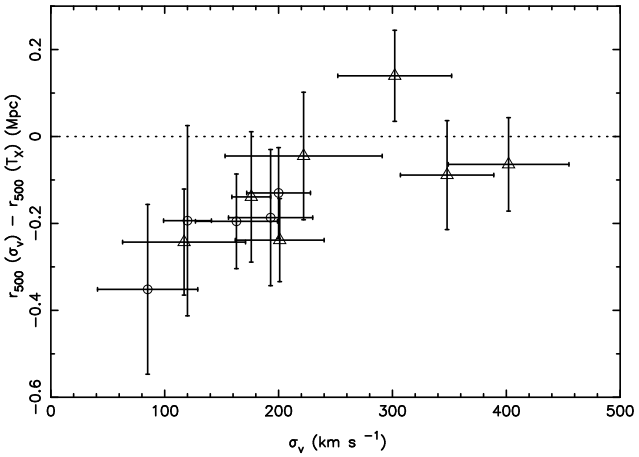

Figure 2. Comparing the r_{500} radius calculated using the velocity dispersion, $r_{500}(\sigma_v)$, and calculated using X-ray temperature, $r_{500}(T_X)$. Groups with intra-group X-ray emission (G-sample) are indicated by the triangles, groups with galaxy-halo emission only (H-sample) by circles - the groups undetected in X-rays do not have T_X measurements. Error bars indicate combined 1σ errors on the r_{500} measurements and 1σ errors on σ_v. The dotted line indicates no difference between the two methods.

$$r_{500}(\sigma_v) = \frac{0.096\sigma_v}{H_0}. \quad (6)$$

The rms error on r_{500} is calculated using standard error propagation. It is also possible to calculate r_{500} as a function of the X-ray temperature, T_X, following Evrard et al. (1996) as,

$$r_{500}(T_X) = \frac{124}{H_0}\sqrt{\frac{T_X}{10}}. \quad (7)$$

Osmond & Ponman (2004) conclude that $r_{500}(T_X)$ is the more robust of the two measures. The two methods of calculating r_{500} are compared in Figure 2 for the 12 groups for which Osmond & Ponman (2004) were able to measure T_X values. The mean difference $\langle r_{500}(\sigma_v) - r_{500}(T_X)\rangle = -0.14 \pm 0.04$. $r_{500}(\sigma_v)$ is smaller than $r_{500}(T_X)$ for the lower velocity dispersion groups, becoming more consistent at $\sigma_v > 200$ km s^{-1}. This suggests that σ_v may be underestimated for these low velocity groups, either due to low group membership or to these groups being less likely to be virialised than the higher velocity dispersion groups. However, as T_X is only available for 12 of the 15 groups, we will use $r_{500}(\sigma_v)$. The conclusions drawn in Section 10 do not change if $r_{500}(T_X)$ is used instead.

The K-band luminosities of the constituent galaxies were summed to calculate the total K-band luminosity of the group, $L_K(Tot)$. Those galaxies without known K magnitudes were assigned $m_K = 13.5$, this has negligible effect on the total calculated as it is dominated by the brightest galaxies. We have also not extrapolated the total luminosity to infinitely small luminosities, however, Girardi et al. (2002) show that this correction is only of the order of 5 per cent. The 1σ error on $L_K(Tot)$ is estimated from the errors on the individual magnitudes from 2MASS.

The mass-to-light ratios were calculated by dividing the virial mass by the sum of the K-band luminosities of the member galaxies. We calculated the rms error on the mass-to-light ratio following standard error propagation analysis.

We obtained morphological T-types for galaxies from the Hyper-Lyon-Meudon Extragalactic DAtabase (HyperLEDA; Paturel et al. 1997). T-types are numerical codes chosen to correspond to morphological galaxy type as defined in the Second Reference Catalogue (RC2; e.g. Corwin et al. 1977). The correspondance with Hubble type is given in more detail in Paturel et al. (1997). In summary, T-types of $-5 \leqslant$ T-type $\leqslant 0$ correspond to E to S0a galaxies whilst $0 <$ T-type $\leqslant 10$ correspond to Sa to Irr galaxy types. We limited these data to those galaxies with magnitudes brighter than the apparent-magnitude limit of the 2MASS catalogue ($m_K \sim 13.1$; Jarrett et al. 2000) at the distance of our furthest group (NGC 3557; $M_K \leqslant -20$) in order to sample the same part of the luminosity function in each group. The early-type fraction, f_{early}, was calculated as the fraction of galaxies in each group with $M_K \leqslant -20$ and T-type $\leqslant 0.0$. The errors were calculated from the poisson errors on these values.

The extent of the group is the maximum projected spatial distance between a group member and the centre of the group.

6 INDIVIDUAL GROUP PROPERTIES

The area of sky around each group in which we collected data are all shown in Appendix B, which also illustrates the extent of the group and hte group members defined by FOF. In this Section we briefly discuss the dynamical properties of each group, based on the values given in Table 3. It is difficult to make a statement as to whether the groups are virialized or not. However, we do assume that groups are dynamically mature if they have bright X-ray emission, above-average velocity dispersion, above-average virial mass, early-type brightest group galaxies (BGGs) and low crossing times (mean values for our sample are given in Table 3).

6.1 NGC 524 Group

This group is in the Northern hemisphere so does not have 6dFGS data available. The group exhibits only galaxy-scale X-ray emission but has an early-type BGG (NGC 524) only 29 kpc and 22 km s^{-1} from the FOF centroid, average velocity dispersion, average mass, crossing time, and a higher than average early-type fraction. These properties suggest that this group is dynamically mature.

6.2 NGC 720 Group

Osmond & Ponman (2004) find this group to have extended intra-group X-ray emission. The brightest galaxy in the group, NGC 720, is an early-type galaxy and is spatially coincident with the centre of the group (within 21 kpc). However, it is offset in velocity by 230 km s^{-1}, nearly twice the velocity dispersion. The other 5 group members are all > 2 magnitudes fainter than NGC 720 itself, suggesting that this could be a fossil group. The X-ray luminosity of the group is just below the fossil group definition of $\log_{10} L_X > 10^{42} h_{50}^{-2}$

erg s^{-1} (Jones et al. 2003). The group has a low mass, however, it also has a high fraction of early-type galaxies consistent with the suggestion that this could be a fossil group.

6.3 NGC 1052 Group

This group shows galaxy-scale X-ray emission associated with the BGG – NGC 1052. NGC 1052 is an elliptical galaxy, offset both kinematically and spatially from the group centre defined by the FOF algorithm. The group consists of 29 members, however its velocity dispersion and virial mass are relatively low and it has a low early-type fraction. Spatially the group is quite extended and irregular, with NGC 1052 lying in a sub-clump which is offset to the group centroid. These properties all suggest that this is a dynamically immature group just coming together for the first time.

6.4 NGC 1332 Group

Brough et al. (2006) concluded, on the basis of its centrally coincident bright lenticular galaxy, few members, average velocity dispersion, low crossing time and high early-type fraction that this is a low-mass, compact, dynamically mature group with a galaxy population similar to that of a much more massive group.

6.5 NGC 1407 Group

Brough et al. (2006) concluded on the basis of its high mass-to-light ratio, high early-type fraction, symmetric intra-group X-ray emission, bright central elliptical galaxy and short crossing time that this structure is a dynamically mature group. This has since been corroborated by Trentham et al. (2006) who came to similar conclusions using deeper observations.

6.6 NGC 1566 Group

This group is an overdensity within the very loose grouping of galaxies in the direction of the Dorado constellation. This grouping is part of the Fornax wall that stretches up through the Fornax cluster to the NGC 1407 and NGC 1332 groups. The group defined by Osmond & Ponman (2004) is centred on NGC 1566 and its galaxy-scale X-ray emission. Kilborn et al. (2005) found 26 members in the group, selected on the basis of cuts in velocity and distance from the position and velocity of NGC 1566, and calculate a velocity dispersion of 282 ± 30 km s^{-1}. The FOF algorithm does not find NGC 1566 to be a member of a group in this field. The BGG is an early-type galaxy – NGC 1553 and is only 29 kpc and 37 km s^{-1} from the FOF centroid. In contrast to Kilborn et al. (2005), the group defined by the FOF algorithm only contains 4 members and has a very low velocity dispersion, and low mass, however, surprisingly it also has a high fraction of early-type galaxies. These properties generally suggest that this group is not dynamically mature.

6.7 NGC 1808 Group

Osmond & Ponman (2004) do not detect X-ray emission $> 3\sigma$ background and define this group to be undetected in X-rays. Its late-type BGG (NGC 1792), few members, low velocity dispersion, low mass and high crossing time indicate that this group is dynamically immature.

6.8 NGC 3557 Group

This group was first found by Klemola (1969) and confirmed by Garcia (1993). Zabludoff & Mulchaey (2000) describe the group as being marginally X-ray detected with a lower number density of galaxies than their other, X-ray detected, groups. However they also find it to have a large number of member galaxies (22) and a high velocity dispersion (282 ± 50 km s^{-1}). They conclude that this group has a much lower dwarf-to-giant galaxy ratio than their other, more X-ray luminous, groups, however it is not possible to verify that here as our data are not deep enough. Osmond & Ponman (2004) find the group to have intra-group X-ray emission. We find the group to have 14 members and a high velocity dispersion, consistent with that measured by Zabludoff & Mulchaey (2000). The early-type BGG (NGC 3557) is only 21 kpc and 171 km s^{-1} from the FOF centroid. In addition to the group's high mass, low crossing time, and high early-type fraction these properties are all consistent with NGC 3557 being a dynamically mature group.

6.9 NGC 3783 Group

Osmond & Ponman (2004) find this group to have group-scale X-ray emission. However, the X-rays only extend to a radius of 69 kpc, and it has a very low X-ray luminosity. Kilborn et al. (2006) suggest that this group may be a very young group. We find its late-type BGG (NGC 3783) 360 kpc and 27 km s^{-1} from the FOF centroid. The low velocity dispersion, mass and low early-type fraction of this group suggest that this group is dynamically immature, in agreement with Kilborn et al. (2006).

6.10 NGC 3923 Group

This group shows galaxy-scale X-ray emission, centred on the BGG, NGC 3923, which is an early-type galaxy lying close (85 kpc and 22 km s^{-1}) to the FOF centroid. The group consists of many members, and has an average velocity dispersion and mass, but a low early-type fraction, suggesting that this group is dynamically immature.

6.11 NGC 4636 Group

This group is also called the NGC 4343 group. The centre of the group defined by Osmond & Ponman (2004) is 3 degrees (0.7 Mpc) south of the centre of the Virgo cluster, however the NGC 4636 group exhibits X-ray luminous intra-group X-ray emission that is distinct from the emission from Virgo. The group does not have 6dFGS data, however, detailed analysis of the region, in particular by SDSS (Abazajian et al. 2003), means that it has a much higher number of galaxies with velocities than do other groups studied, but few with K-magnitudes. Using the same FOF technique as used for the other groups therefore fails in this region. The extra depth of sources results in confusion between this group and the Virgo cluster and a FOF analysis

with all galaxies determines a group that is indistinguishable from Virgo.

For this region we therefore cut the data by the apparent magnitude limit of 2MASS ($K \leqslant 13.1$ mag) to perform the FOF analysis. This defines a group that is distinct from the Virgo cluster, as suggested by its X-ray emission. The early-type galaxy NGC 4636 is the brightest galaxy in the group, close to the FOF centroid (within 87 kpc and 38 km s^{-1}) and, given the apparent-magnitude cut, has a large number of members, average velocity dispersion and high mass. On balance, these properties suggest that this group is dynamically mature.

6.12 NGC 5044 Group

Osmond & Ponman (2004) show this group to have group-scale X-ray emission and it is the most X-ray luminous group in our sample – putting it on the border of cluster-mass scales. Its large size means that it has been the subject of much study. Most recently, Cellone & Buzzoni (2005) have analysed the group in detail, finding a group of 27 members with a velocity dispersion $\sigma_v = 431$ km s^{-1}.

The large elliptical, NGC 5044, is the brightest galaxy in the group and is 91 kpc and 156 km s^{-1} from the FOF centroid. Our velocity dispersion is consistent with that of Cellone & Buzzoni (2005). This is a classically dynamically mature group with many members, high velocity dispersion, high mass, high early-type fraction and a low crossing time.

6.13 HCG 90

This group was first found by Klemola (1969) and then defined as a Hickson Compact Group (HCG) by Hickson (1982). Maia et al. (1989) established that this group extends well beyond the compact nucleus examined by Hickson (1982). Zabludoff & Mulchaey (1998) found that this is in fact a massive group consisting of 16 members with a high velocity dispersion (293 ± 36 km s^{-1}) and extended X-rays. The three central galaxies (NGC 7173, NGC 7174, and NGC 7176) appear to be interacting, although they are dominated in luminosity by the elliptical NGC 7176 which appears to be undisturbed. Longo et al. (1994) illustrate that NGC 7176 and NGC 7174 are not actually interacting and that this is in fact a projection effect. We find the elliptical galaxy NGC 7176 to be the BGG. It lies only 33 kpc and 84 km s^{-1} from the FOF centroid. We find the group to consist of many members, and it has a low crossing time and an average velocity dispersion, however it has a low early-type fraction suggesting that it might still be dynamically immature.

6.14 IC 1459 Group

Osmond & Ponman (2004) find this group to have extended intra-group X-ray emission. We find the group to have an early-type BGG – IC 1459 is 32 kpc and 153 km s^{-1} from the FOF centroid. The group has few members and a high velocity dispersion, high virial mass, high mass-to-light ratio but a lower than average early-type fraction. These properties generally suggest that this group is a dynamically mature group structure.

6.15 NGC 7714 Group

Osmond & Ponman (2004) find the X-ray emission of this group to be $< 3\sigma$ background, it is therefore, undetected in X-rays. This group is in the Northern hemisphere and does not therefore have 6dF data. The group defined by FOF does not contain NGC 7714. The BGG (NGC 7716) is a late-type galaxy, only 10 kpc and 26 km s^{-1} from the FOF centroid. The group has very few members (4, and only 1 with a measured K-magnitude), very low velocity dispersion, very low mass, and no early-type galaxies. This all suggests that this group is not dynamically mature.

6.16 Summary

The properties of these groups depend strongly on their X-ray luminosities. The groups with the highest X-ray luminosities have the highest masses and early-type BGGs that lie close to the FOF defined centroid (Section 9). They also have the most members, highest velocity dispersions, and low crossing times and high early-type fractions. Although these groups generally have extended intra-group X-ray emission, there are some showing only galaxy halo X-ray emission.

In contrast, those groups with the lowest and undetected X-ray luminosities have low masses and velocity dispersions and they generally have fewer members than those groups with the highest X-ray luminosities. The properties of the NGC 3783 group are consistent with these groups, despite its marginally extended X-ray emission.

These differences suggest that the X-ray luminosity of these groups is more closely related to their dynamical properties than whether or not the groups show extended or halo X-ray emission, as defined by Osmond & Ponman (2004).

7 STATISTICS

In the relationships presented below we calculated Kendall's rank correlation probabilities for each group parameter pair using the IRAF/STSDAS/STATISTICS package routine. Kendall's rank correlation was used because it is more reliable for samples where $N < 30$ than the Spearman rank correlation. It is also non-parametric – Helsdon & Ponman (2000) show that the scatter in the properties of groups is intrinsic rather than statistical so it is appropriate not to take the statistical errors into account in the correlation.

Two of the groups only have upper limits for their X-ray luminosities. The survival analysis tasks available in IRAF can take this into account in the correlation. Survival analysis tasks are discussed in more detail in O'Sullivan et al. (2001). In summary, survival analysis assumes that the upper limits provided hold only limited information regarding the true values of the X-ray luminosities of these groups. We take the uncensored parameter as the independent variable and the censored parameter (i.e. X-ray luminosity) as the dependent parameter.

We also use the Buckley-James algorithm available in the same package to fit straight lines to our data. The Buckley-James method is also non-parametric, using the Kaplan-Meier estimator for the residuals to calculate the regression, and can also take censored data into account. As

for the correlation, we take the uncensored parameter as the independent variable and the censored parameter (i.e. X-ray luminosity) as the dependent parameter.

8 SCALING RELATIONS

Diffuse X-rays are emitted by a hot plasma trapped in the gravitational potential of a galaxy, group or cluster. The X-ray luminosities of groups of galaxies are therefore a measure of the hot gas in the system and it is interesting to determine how the gas properties correlate with the properties of the galaxies that share the same potential well.

Assuming that the evolution of groups and clusters is solely due to their collapse under gravity, groups are simply scaled down clusters. This 'self-similar' model predicts that X-ray luminosity is proportional to the velocity dispersion of member galaxies: $L_X(Bol) \propto \sigma_v^4$ (e.g. Quintana & Melnick 1982). Previous research on clusters (e.g. Mahdavi & Geller 2001; Hilton et al. 2005) has resulted in $L_X(Bol) \propto \sigma_v^{4.8\pm0.7}$ (Hilton et al. 2005). Although this does not rule out simple, self-similar evolution, it is also consistent with feedback processes (i.e. heating by non-gravitational processes) being significant.

One of the main observational signatures of non-gravitational processes is a steepening of the X-ray relationships in the group regime (e.g. Borgani et al. 2004). Hence, it is also important to examine the relationships followed by groups. Previous analysis of groups reveals that the $L_X - \sigma_v$ relation does not steepen in group-sized systems, with a growing consensus that groups are consistent with the cluster relationship (Mulchaey & Zabludoff 1998; Helsdon & Ponman 2000; Mahdavi & Geller 2001 and T. Ponman, private communication 2005). We observe a 99.96 per cent correlation between these properties (Figure 3) and, using the Buckley-James algorithm described above, find a relationship for all 15 groups of

$$\log_{10} L_X(r_{500}) = 3.11^{\pm0.59} \log_{10} \sigma_v + 34.38, \quad (8)$$

with a standard deviation on the regression of 0.40. This is close to the prediction of self-similarity. However, Osmond & Ponman (2004) discuss the biases in their L_X calculation which lead to a flattening of this relationship. As we use their X-ray luminosities these biases are also present in this sample, leading to uncertainty in the true value of this relationship.

Self-similarity predicts that the X-ray emitting gas is bound to groups with a mass proportional to the virial mass – $M_V \propto T_X^{3/2}$ (Borgani et al. 2004). $L_X \propto T_X^2$, therefore $L_X \propto M_V^{4/3}$. Figure 4 illustrates the close relationship we observe between these parameters – correlated at the 99.91 per cent level. Using the Buckley-James algorithm described above we find a relationship for all 15 groups of

$$\log_{10} L_X(r_{500}) = 1.13^{\pm0.27} \log_{10} M_V + 26.48, \quad (9)$$

with a standard deviation on the regression of 0.48. This is consistent with the prediction of self-similarity.

Early-type fractions in clusters are observed to correlate strongly with L_X (Edge & Stewart 1991). In groups, Zabludoff & Mulchaey (1998) found a strong correlation of early-type fraction with velocity dispersion. They also found

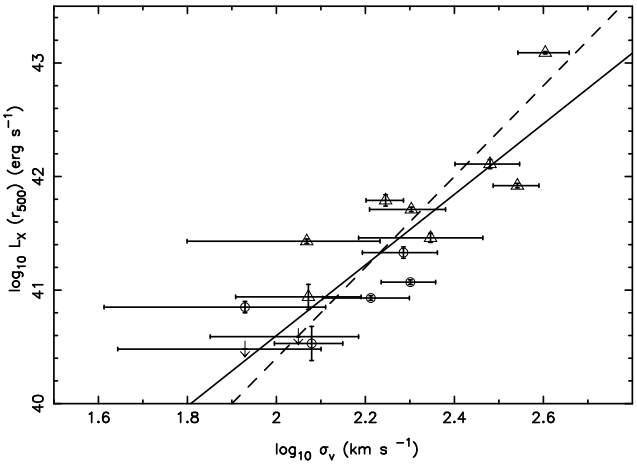

Figure 3. The relationship between $L_X(r_{500})$ and σ_v. Groups with intra-group X-ray emission (G-sample) are indicated by the triangles, groups with galaxy-halo emission only (H-sample) by circles and groups undetected in X-rays (U-sample) by their upper-limit. Error bars indicate 1σ errors. The dashed line indicates the self-similar prediction whilst the solid line indicates the regression line fit given by Equation 8.

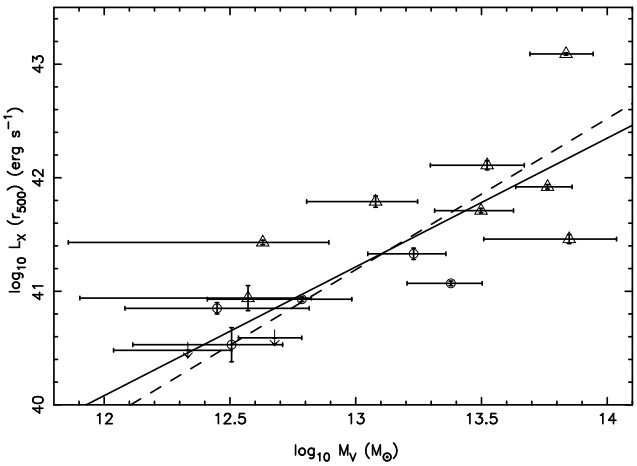

Figure 4. The relationship between the X-ray luminosity $L_X(r_{500})$ and the virial mass, M_V. G-sample galaxies are indicated by triangles, H-sample by circles and U-sample groups by upper limits. Error bars indicate 1σ errors. The dashed line indicates the self-similar prediction whilst the solid line indicates the regression line fit given by Equation 9.

no early-type galaxies in the 3 groups without observed X-ray emission and early-type fractions up to those observed in clusters ($f_{early} \sim 0.55 - 0.65$; Whitmore et al. 1993) in their 9 groups with observed X-ray emission ($0.25 < f_{early} < 0.55$). We also find three of our groups (NGC 1808, NGC 3783 and NGC 7714) to have no early-type galaxies. There is no X-ray emission associated with the NGC 1808 or NGC 7714 groups, similar to the Zabludoff & Mulchaey (1998) groups with no early-type galaxies, however the NGC 3783 group shows marginally extended X-ray emission, characteristic of intra-group gas. This group is shown in Section 6.9 and by Kilborn et al. (2006) to be a young group in the process of forming, consistent with this low early-type fraction.

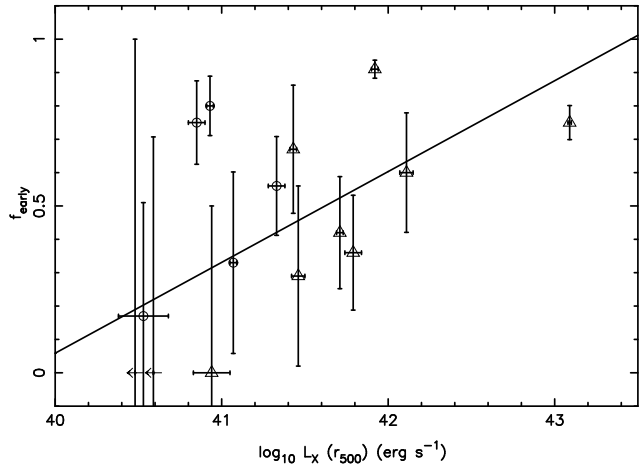

Figure 5. The fraction of early-type galaxies, f_{early}, in each group with respect to the group X-ray luminosity $L_X(r_{500})$. G-sample galaxies are indicated by triangles, H-sample by open circles and U-sample groups by upper limits. Error bars indicate 1σ errors on the X-ray luminosities and poisson errors on the early-type fractions. The solid line indicates the regression line fit given by Equation 10.

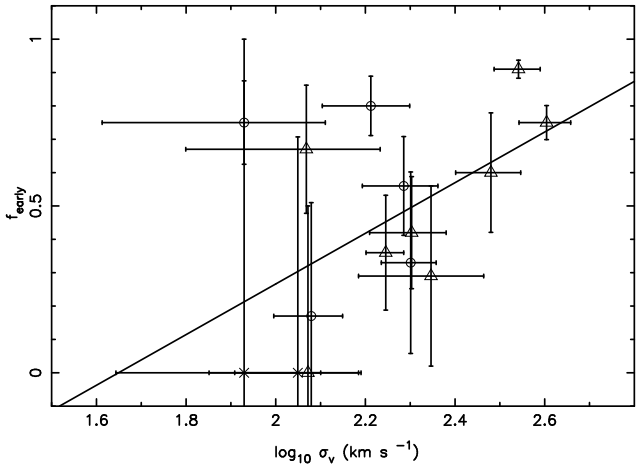

Figure 6. The relationship between the fraction of early-types, f_{early}, in each group and the velocity dispersion, σ_v. G-sample galaxies are indicated by triangles, H-sample by open circles and U-sample groups by crosses. Error bars indicate 1σ errors on the velocity dispersions and poisson errors on the early-type fractions. The solid line indicates the regression line fit given by Equation 11.

Osmond & Ponman (2004) and Wilman et al. (2005) find weaker trends with early-type fraction. We find the early-type fraction to be correlated with L_X (95.87 per cent correlation, Figure 5) and σ_v (90.98 per cent correlation; Figure 6). Fitting to these data using the Buckley-James algorithm we find:

$$f_{early} = 0.27^{\pm 0.11} \log_{10} L_X(r_{500}) - 10.8, \quad (10)$$

and,

$$f_{early} = 0.76^{\pm 0.35} \log_{10} \sigma_v - 1.2. \quad (11)$$

These relationships are illustrated in Figures 5 and 6.

In Section 6 we concluded that the X-ray luminosity of the groups provides more information on the optical properties of these groups than the extent of their X-ray emission. This conclusion is supported here, with X-ray luminosity highly correlated with velocity dispersion, virial mass, and the morphologies of the group members.

8.1 Mass-to-Light Ratio

The ratio of mass-to-light in a system represents a proxy for the efficiency with which stars are formed within haloes of different masses. Previous studies have used group dynamical masses (e.g. Carlberg et al. 2001; Girardi et al. 2002; Eke et al. 2004b), comparison of the theoretical mass function with the observed luminosity function (Marinoni & Hudson 2002), mass measurements from weak lensing (e.g. Parker et al. 2005) and the fundamental plane (Zaritsky et al. 2006) to examine mass-to-light ratios. There is a growing consensus that mass-to-light ratios reach some minimum at a system mass of $\sim 10^{12} M_\odot$ (e.g. Marinoni & Hudson 2002; Eke et al. 2004b; Zaritsky et al. 2006) and rise steadily through group-sized systems (Carlberg et al. 2001; Girardi et al. 2002; Marinoni & Hudson 2002; Eke et al. 2004b; Parker et al. 2005; Zaritsky et al. 2006). However there is some disagreement on cluster mass scales with Sanderson & Ponman (2003) and Eke et al. (2004b) observing no relationship of mass-to-light ratio with cluster mass whilst Girardi et al. (2002) and Zaritsky et al. (2006) do.

Using the virial masses and total K-band luminosities calculated for our groups, we show the relationship of the mass-to-light ratio with mass in Figure 7. The mass-to-light ratio clearly increases with system mass. Using the Buckley-James algorithm we find a relationship of

$$\log_{10}(M_V/L_K) = 0.65^{\pm 0.12} \log_{10} M_V - 6.8, \quad (12)$$

This is similar to the relationship determined by Eke et al. (2004b) and Parker et al. (2005) but steeper than the $M/L_B \propto M^{0.33}$ measured by Marinoni & Hudson (2002).

However, Girardi et al. (2002) and Eke et al. (2004b) indicate the pitfalls of working with correlated quantities. We therefore follow Girardi et al. (2002) and examine the more robust relationship between mass and light, presented in Figure 8. The scatter in this relationship is evident. We therefore fit both $M_V \propto L_K$ and the inverse, $L_K \propto M_V$, and use the difference between these fits as an estimate of the error on the fit. Using the Buckley-James algorithm we find a bisecting relationship of,

$$\log_{10} M_V = 2.0^{\pm 0.9} \log_{10} L_K(Tot) - 9.4. \quad (13)$$

In Figure 8 we also indicate the $M_V \propto L_K$ relationship and the Girardi et al. (2002) fit to their data: $M_V \propto L_B^{1.338 \pm 0.033}$. The slope fitted here is consistent with that of Girardi et al. (2002) and with mass increasing faster than luminosity.

9 BRIGHTEST GROUP GALAXIES

Hierarchical structure formation predicts that the galaxy at the centre of a dark-matter halo will continue growing as it accretes other galaxies and that it will grow at

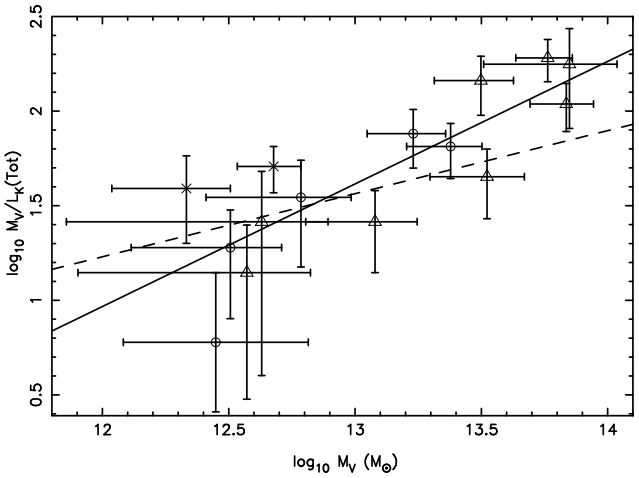

Figure 7. The relationship between the mass-to-light ratio and the virial mass of the group. G-sample galaxies are indicated by triangles, H-sample by circles and U-sample groups by crosses. The error bars give the 1σ errors. The solid line indicates the regression line fit to all 15 groups given by Equation 12, whilst the dashed line is the relationship of Marinoni et al. (2002).

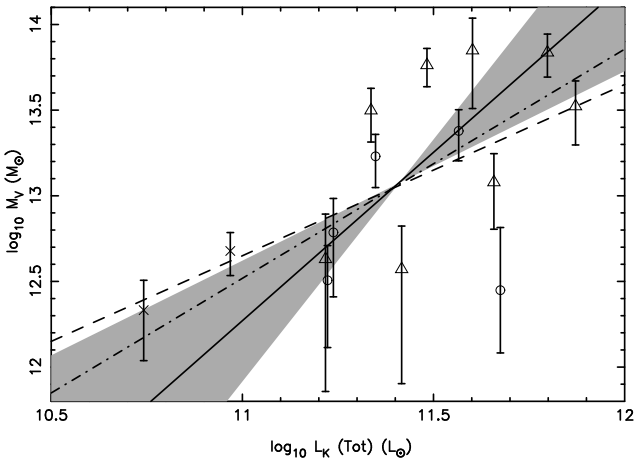

Figure 8. The relationship between the virial mass of the group and its total luminosity. G-sample galaxies are indicated by triangles, H-sample by circles and U-sample groups by crosses. The error bars give 1σ errors on M_V, the 1σ errors on the total K-band luminosities are of the order of the size of the points and are not therefore plotted. The dashed line indicates the simple $M_V \propto L_K$ line, the dot-dashed line the relationship of Girardi et al. (2002), whilst the shaded areas indicate the direct and inverse fits and the solid line gives the bisecting fit (Equation 13).

the expense of other galaxies. It is, therefore, expected to be the brightest, most massive galaxy in the halo at all times. In this paradigm the bright elliptical galaxies found at the centres of clusters (Brightest Cluster Galaxies; BCGs; e.g. Brough et al. 2002, 2005) form in the group environment and as the groups merge to form clusters, newly accreted massive galaxies will sink to the centre of the potential well by dynamical friction and merge with the central galaxy. Groups with extended X-ray emission are frequently observed with bright, early-type galaxies at the centre of their X-ray emission, similar to the BCGs observed at the centres of clusters (Zabludoff & Mulchaey 1998; Osmond & Ponman 2004). If the hierarchical picture of structure formation is correct then these brightest group galaxies (BGGs) can be seen as evolutionary tracers of the system (Zabludoff & Mulchaey 1998; Brough et al. 2002; Lin & Mohr 2004).

Here, the BGGs were selected as the galaxy with the brightest K-magnitude within $\pm 2\sigma_v$ of the mean group velocity. The BGGs are detailed in Table 4. Of 8 groups with extended X-ray emission in this sample, 7 have early-type BGGs. The exception is the NGC 3783 group, which is shown in Section 6.9 and by Kilborn et al. (2006) to have properties which are consistent with this group still being in the process of relaxation.

Comparing the magnitude distribution of early- and late-type BGGs we found that the early-type BGGs are more luminous than the late-type BGGs, as also seen by Osmond & Ponman (2004). A Kolmogorov-Smirnov (KS) test gives a probability of only 3.0 per cent that the early and late-type BGGs are drawn from the same parent population.

The hierarchical structure formation paradigm predicts that the brightest galaxy in a halo will lie at rest with respect to the potential well. It is therefore interesting to examine whether BGGs lie at rest with respect to the spatial and velocity centroids of their groups. Previous studies have found that 90 per cent of BCGs lie within $0.38r_{200}$ of their cluster centroid (Lin & Mohr 2004). Zabludoff et al. (1990) and Oegerle & Hill (2001) find significant departures in the velocities of BCGs from the mean cluster velocity but within the mean velocity dispersion of their clusters.

In the group environment, Mulchaey & Zabludoff (1998) found that the BGGs of their X-ray detected groups lie within $5 - 10h^{-1}$ kpc of the X-ray peak of their groups.

We examine the offset of the BGG from the group luminosity-weighted centroid and mean group velocity, scaled by the size and velocity dispersion of the group. (Figure 9). There are four clear outlying BGGs in Figure 9. These BGGs are all in groups showing signs of being dynamically immature: NGC 3783 is a late-type galaxy lying close to the FOF centroid in velocity ($0.1\sigma_v$), but it is offset by $2.2r_{500}$ spatially. Despite this it is still the closest galaxy to the FOF centroid in this group. This group was determined by Kilborn et al. (2006) and in Section 6.9 to still be in the process of forming. NGC 1792 is also a late-type galaxy and is offset by $1.3\sigma_v$ in velocity with respect to its group centroid. This group (NGC 1808) was determined in Section 6.7 to be dynamically immature. NGC 1052 is an early-type galaxy but it lies at both significant radius ($0.9r_{500}$) and velocity ($1.6\sigma_v$) from the FOF centroid. This group only has X-rays associated with NGC 1052 itself and the group was shown in Section 6.3 to be relaxing for the first time. Spatially, NGC 720 lies close to the FOF centroid, but is offset by nearly $2\sigma_v$ in velocity. If this group is a fossil group then it should have reached dynamical equilibrium. The observation that the BGG is offset in velocity by $2\sigma_v$ therefore suggests that this might not be a fossil group.

All BGGs in dynamically mature groups lie within a group-centric radius of $\sim 0.35r_{500}$ and $\pm 0.6\sigma_v$ in velocity of their FOF centroid. These groups all have high X-ray luminosities, consistent with the sample of Mulchaey & Zabludoff (1998). We conclude that it is only

Table 4. Properties of Brightest Group Galaxies (BGGs).

Group	BGG	M_K (mag)	$L_K(BGG)$ ($10^{11} L_\odot$)	$\|R- < R > \|$ (kpc)	$\frac{\|R-<R>\|}{r_{500}}$	$v - \bar{v}$ (km s^{-1})	$\frac{v-\bar{v}}{\sigma_v}$	$M_{K,1} - M_{K,2}$ (mag)	Type
NGC 524	NGC 0524	-24.53±0.01	1.33±0.02	29	0.11	-22	-0.11	1.73±0.03	E
NGC 720	NGC 0720	-24.66±0.02	1.50±0.02	21	0.13	230	1.97	2.95±0.04	E
NGC 1052	NGC 1052	-23.78±0.01	0.67±0.01	144	0.87	185	1.54	0.51±0.02	E
NGC 1332	NGC 1332	-24.48±0.02	1.27±0.02	42	0.19	50	0.31	1.70±0.03	E
NGC 1407	NGC 1407	-24.77±0.02	1.66±0.03	95	0.20	92	0.26	1.43±0.03	E
NGC 1566	NGC 1553	-25.26±0.02	2.61±0.04	29	0.25	-37	-0.44	0.53±0.02	E
NGC 1808	NGC 1792	-24.07±0.02	0.87±0.01	25	0.16	149	1.33	3.25±0.07	L
NGC 3557	NGC 3557	-25.90±0.02	4.70±0.07	21	0.05	171	0.57	1.73±0.02	E
NGC 3783	NGC 3783	-24.12±0.02	0.91±0.02	360	2.24	-9	-0.08	0.07±0.02	L
NGC 3923	NGC 3923	-25.02±0.02	2.09±0.03	85	0.31	-22	-0.11	1.12±0.02	E
NGC 4636	NGC 4636	-24.05±0.02	0.86±0.01	87	0.32	38	0.19	0.84±0.03	E
NGC 5044	NGC 5044	-24.49±0.02	1.28±0.02	91	0.16	156	0.39	0.76±0.03	E
HCG 90	NGC 7176	-24.70±0.02	1.56±0.03	33	0.14	-84	-0.48	0.30±0.03	E
IC 1459	IC 1459	-25.24±0.02	2.56±0.04	28	0.09	-107	-0.48	1.98±0.03	E
NGC 7714	NGC 7716	-23.51±0.03	0.52±0.01	10	0.09	-26	-0.31	4.04±0.10	L
Mean Values		-24.57 ± 0.16	3.19±0.50					1.53 ± 0.30	

The columns indicate (1) Group name; (2) BGG name; (3) Absolute K-band magnitude of BGG with 1σ error; (4) Luminosity of BGG with 1σ error; (5) Offset of BGG with respect to luminosity-weighted group centroid; (6) Offset of BGG with respect to luminosity-weighted group centroid scaled by group r_{500} radius; (7) Offset of BGG velocity with respect to mean group velocity; (8) Offset of BGG velocity with respect to mean group velocity, scaled by group velocity dispersion; (9) Magnitude difference between first and second ranked galaxies with 1σ error; (10) Morphology of BGG: E for early-type (T-type $\leqslant 0.0$) and L (T-type > 0.0) for late-type galaxies. The final row gives the means and error on the mean ($\sigma/\sqrt{N}$) of these quantities.

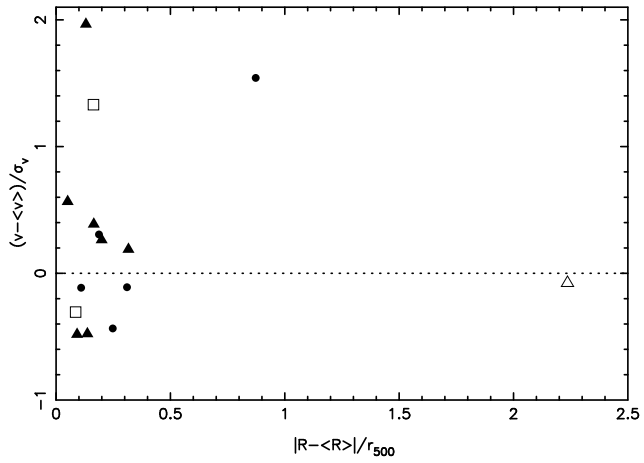

Figure 9. The relationship between the offset of the BGG in position and velocity with respect to the luminosity-weighted centroid and the mean velocity determined by FOF. The symbols indicate early-type (closed points) and late-type (open point) BGGs, with those in G-sample groups as triangles, in H-sample groups as circles and those in U-sample groups are marked by squares.

safe to assume that the brightest galaxy in the group lies at rest with respect to its potential well once the group has come into equilibrium.

Brough et al. (2002) found that the K-band aperture magnitudes of BCGs at low redshifts ($z < 0.1$) are only weakly correlated with the X-ray luminosity of their host cluster. In contrast, Osmond & Ponman (2004) find a 6σ correlation between BGG luminosity and $L_B(Tot)$ and a 2.5σ correlation with group X-ray luminosity. Here we find a 99.87 per cent correlation with total K-band luminosity (Figure 10) and a 95.82 per cent correlation with X-ray luminosity (Figure 11). The fact that the BGG luminosity is more correlated with total group luminosity reflects the dependence of $L_K(Tot)$ on $L_K(BGG)$. Therefore, we can state that, to first order, there is a decrease in the dependence of the luminosity of the central galaxy on its host halo mas between groups and clusters. This has been predicted analytically by Cooray & Milosavljević (2005) who show that above a critical halo mass of $\sim 1-6\times10^{13} M_\odot$, the timescale on which dynamical friction induces orbital decay in the accreted galaxies exceeds the age of the dark-matter halo. As a result of this the relationship between central galaxy luminosity and host halo mass turns over at this critical mass, albeit with some scatter. The groups studied here lie close to this critical mass range and lie within the scatter. Therefore, in a future paper we will compare the properties of all the GEMS BGGs with those of the BCGs of Brough et al. (2002) in order to explore a significantly wider halo mass range and fully investigate this prediction.

A result of the prediction by Cooray & Milosavljević (2005) is that the fraction of total group light in the BGG will decrease with increasing mass of the group. Lin & Mohr (2004) observe this relationship on cluster mass scales, with BCGs constituting 40–50 per cent of total light at poor-cluster mass scales, down to 5 per cent at rich-cluster mass scales. We observe a continuation of that effect here to very poor groups where the brightest galaxy makes up > 90 per cent of the total group luminosity (Figure 12).

In the hierarchical structure formation paradigm, the total luminosity of the group is expected to rise as the group accretes galaxies, such that the correlations between group mass, total K-band luminosity and X-ray luminosity are re-

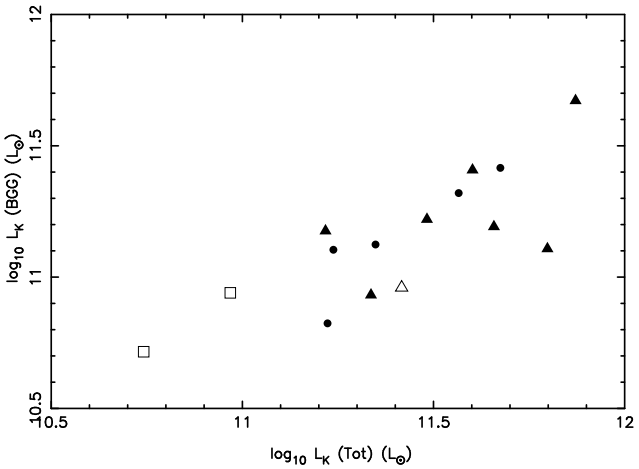

Figure 10. The relationship between the K-band luminosity of the BGG, $L_K(BGG)$, and the total K-band luminosity of the group, $L_K(tot)$. The symbols indicate early-type (closed points) and late-type (open point) BGGs, with those in G-sample groups as triangles, in H-sample groups as circles and those in U-sample groups are marked by squares. The 1σ errors on the BGG and total K-band luminosities are of the order of the size of the points and are not therefore plotted.

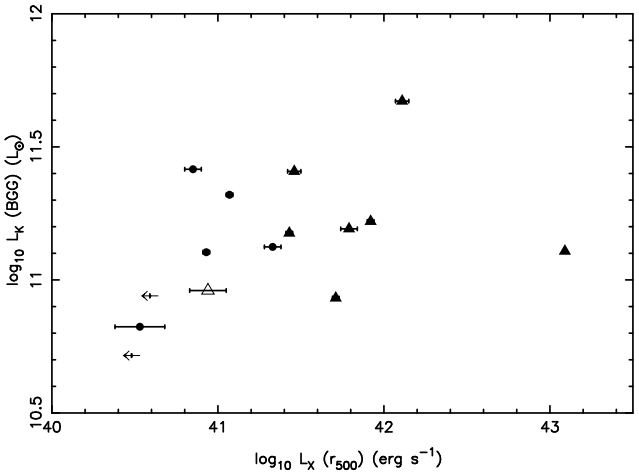

Figure 11. The relationship between the K-band luminosity of the BGG, $L_K(BGG)$, and the X-ray luminosity, $L_X(r_{500})$ of its host group. The symbols indicate early-type (closed points) and late-type (open point) BGGs, with those in G-sample groups as triangles, in H-sample groups as circles and those in U-sample groups (both late-types) are marked by upper-limits. The error bars indicate 1σ errors on the X-ray luminosities. The 1σ errors on the K-band luminosity of the BGG are of the order of the size of the points and are not therefore plotted.

tained. The correlation of the luminosity of the BGG with the total luminosity of the group (Figure 10) then means that the BGGs themselves must have also accreted galaxies. However, the dynamical time required for the accreted galaxies to fall in and merge with the central galaxy increases with increasing group mass. Above the critical mass predicted by Cooray & Milosavljević (2005) the accreted galaxies have not had time to merge with the central galaxy, such

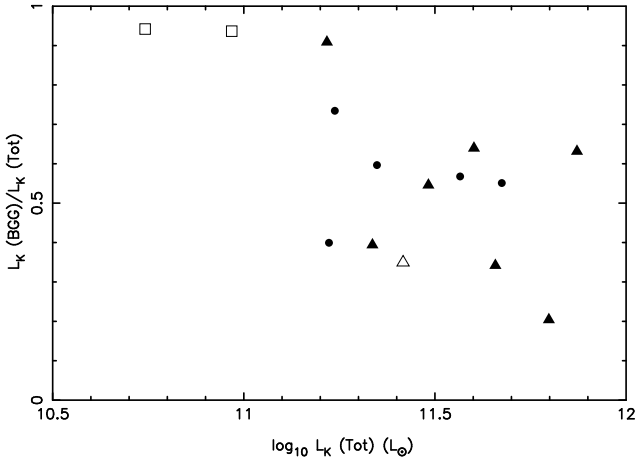

Figure 12. The relationship between the ratio of the K-band luminosity of the BGG, $L_K(BGG)$, and the total K-band luminosity of the group, $L_K(Tot)$ and $L_K(Tot)$. The symbols indicate early-type (closed points) and late-type (open point) BGGs, with those in G-sample groups as triangles, in H-sample groups as circles and those in U-sample groups are marked by squares. The 1σ errors on the BGG and total K-band luminosities are of the order of the size of the points and are not plotted.

that the fraction of group light in the BGG falls with increasing total group luminosity.

The accretion of galaxies by the group, that are not cannibalized by the BGG, will also affect the dominance of the BGG over the second brightest galaxy in the group. We only observe a weak correlation with total light of galaxies in the system (90.79 per cent), consistent with Osmond & Ponman (2004), Lin & Mohr (2004) and Miles et al. (2004). However, the mean offset $\langle M_{K,1} - M_{K,2} \rangle = 1.53 \pm 0.30$ mag, is significantly higher than Lin & Mohr (2004) who find $\langle M_{K,1} - M_{K,2} \rangle = 0.66 \pm 0.48$ mag in their sample of 93 BCGs. The increase in domination of the BGG into the group environment is consistent with Loh & Strauss (2006) who find the dominance of BCGs to be more prominent in group-like environments than in cluster-like environments. The observation that BGGs are more dominant in the group environment than in the cluster environment adds evidence to the merging picture in which larger groups have accreted more galaxies but the BGG has yet to absorb the accreted members.

9.1 Summary

The BGGs of all the dynamically mature groups are early-type galaxies and lie within a group-centric radius of $0.3r_{500}$ and $\pm 0.6\sigma_v$ in velocity of the FOF centroid. They are significantly brighter than the late-type BGGs.

The luminosity of the BGGs increases with increasing total K-band luminosity and X-ray luminosity of the group. However, the fraction of group light in the BGG and the dominance of the BGG over the second brightest galaxy fall with increasing total group luminosity. These properties are all consistent with the paradigm in which BGGs grow by mergers at early times in group evolution while the group continues to grow by accreting infalling galaxies.

10 A COMPOSITE GROUP

The numbers of galaxies in each of our groups are few. Therefore, in order to study the group-wide properties statistically it is necessary to stack the galaxies in each group to construct a composite group. To sample the same portion of the luminosity function of each group we cut the sample by absolute magnitude, based on the apparent-magnitude limit of 2MASS (i.e. $m_K < 13.1$; Jarrett et al. 2000) at the distance of the furthest group (NGC 3557), $M_K \leqslant -20$ mag. This creates a composite group with 113 galaxies.

Owing to the size and number of regions studied it was unfeasible to obtain new photometric data. We therefore used HyperLEDA to obtain total B-band magnitudes and morphological T-types for the absolute magnitude-limited sample. This resulted in 112 galaxies with both B-band magnitudes and T-types.

We also used the dataset to construct a field sample. Galaxies within $\pm 2\sigma_v$ of the group defined by FOF, which were not defined to be members of that group *or* other groups in the same field, were selected to be field galaxies. The velocity range was chosen such that galaxies in the same velocity range of the group would be at the same distance so that accurate absolute magnitudes could be calculated. Above the absolute magnitude limit this gives 161 field galaxies, of which 157 have both B-band magnitudes and T-types.

10.1 Velocity Dispersion Profile

The line-of-sight velocity dispersion as a function of the projected group-centric distance provides information on the velocity anisotropy of galaxy orbits. Clusters generally have falling velocity dispersion profiles with radius, consistent with isotropic galaxy orbits (e.g. Carlberg et al. 1997; Girardi et al. 2002; Łokas & Mamon 2003). However, at group scales Carlberg et al. (2001) observed a rise in the projected velocity dispersion with radius. Using this to examine the mass-to-light profile of their groups they concluded that galaxies contract within their dark matter haloes by dynamical friction. In contrast, Zabludoff & Mulchaey (1998); Girardi et al. (2002) and Parker et al. (2005) observed falling velocity dispersion profiles in their group samples, which are consistent with clusters.

We have scaled our galaxy data by their group velocity dispersion and group size (as measured by their r_{500} radius), binned the galaxies into equal number bins and applied the gapper algorithm (Equation 2) to calculate robust velocity dispersions. The corresponding errors are estimated using the jackknife algorithm. The velocity dispersion profile of our composite group, illustrated in Figure 13, extends to a radius $> 2r_{500}$, much further than previous studies. We observe that the velocity dispersion profile falls with radius. The large error bars mean that it is not possible to determine any possible velocity anisotropy of the galaxy orbits with these data, however they are consistent with isotropic orbits.

10.2 Magnitudes

Miles et al. (2004) obtained deep B and R-band photometry of 25 GEMS groups and found a difference in the luminosity function (LF) of galaxies in groups with X-ray luminosities $\log_{10} L_X(Bol) < 41.7$ erg s^{-1} in comparison to the LF of galaxies in groups with X-ray luminosities greater than this. They found a dip at $-19 < M_B < -17$ ($-20.5 < M_K < -23$) in the LF of galaxies in groups with low X-ray luminosities, mainly associated with the early-type galaxies. They concluded that the dip is a result of current rapid dynamical evolution in the low X-ray luminosity groups.

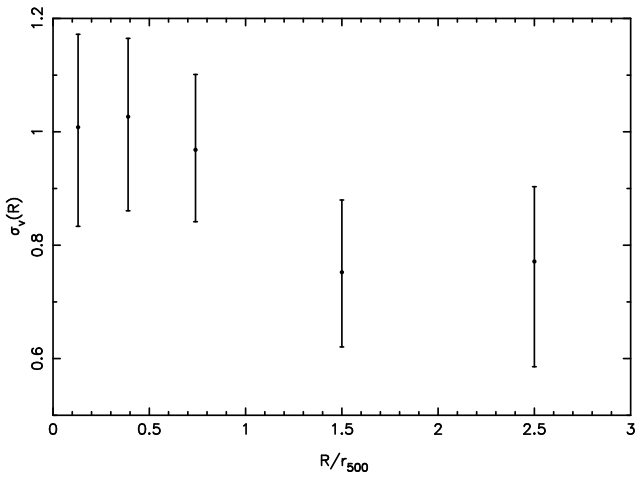

Figure 13. The line-of-sight velocity dispersion, $\sigma_v(R)$ as a function of the scaled projected group-centric distance, R/r_{500}, of our composite group. The error bars indicate 1σ errors on the velocity dispersions.

Our sample has advantages over that of Miles et al. (2004) in that all of our galaxies are spectroscopically confirmed as group members, our stacked group extends to larger radii ($2r_{500}$ in comparison to the $0.3r_{500}$ of Miles et al. (2004)) and we also have a field sample with which to compare our group properties. However, we only study 15 groups to $M_K = -20$ so the data is too shallow to conclusively examine the LF of this sample, or further divide the sample by galaxy morphology.

We examine the radial dependence of the magnitudes of the galaxies in our sample in Figure 14. We divide the sample into high and low-L_X groups by the X-ray luminosity at which Miles et al. (2004) observe a separation in the galaxy populations: $\log_{10} L_X(r_{500}) = 41.7$ erg s^{-1}.

Our composite group indicates that the mean galaxy magnitude fades with distance from the group centre. We also see that the mean magnitudes of the galaxies in high X-ray luminosity groups are fainter than those in low X-ray luminosity groups. This is in contrast to Miles et al. (2004) who observed that the total B-band luminosity within a radius of $0.3r_{500}$ is lower and more concentrated in low-L_X groups. However, our result is consistent with observations that the ratio of dwarf-to-giant galaxies increases with group mass (Ferguson & Sandage 1991; Zabludoff & Mulchaey 2000; Wilman et al. 2005; Cellone & Buzzoni 2005). We explicitly examine this by calculating the number of galaxies with $M \leqslant M^\star$ ('giants'; $M^\star = -22.6$; Kochanek et al. 2001) and $M > M^\star$ ('dwarfs') in high- and low X-ray luminosity groups. We find dwarf-to-giant ratios of 1.71 ± 0.27 in high-L_X groups and 0.96 ± 0.2 in low X-ray luminosity groups, where the errors given are the poisson errors on these quan-

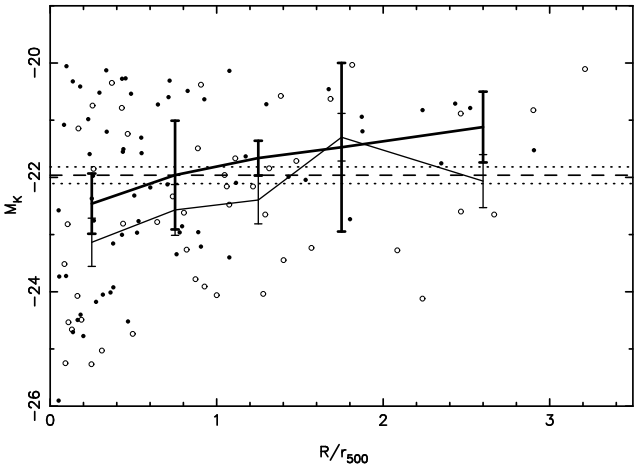

Figure 14. The relationship of M_K with scaled group radius. The solid points indicate galaxies in high-L_X groups ($\log_{10}L_X(r_{500}) > 41.7$ erg s^{-1}) and open points indicate galaxies in low-L_X groups ($\log_{10}L_X(r_{500}) < 41.7$ erg s^{-1}). The solid line indicates the mean luminosity at each radius for high-L_X groups (thick black line) and low-L_X groups (thin black line), whilst the error bars show the error on the mean magnitude. The dashed line shows the mean luminosity in our field sample and the dotted lines indicate the error on this mean value.

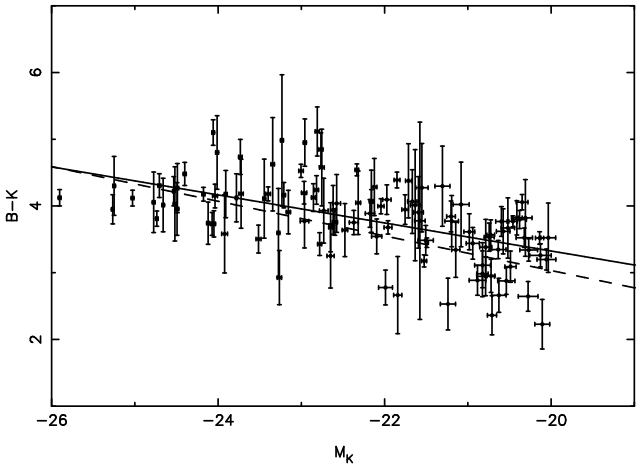

Figure 15. $B-K$ vs M_K colour-magnitude diagram. The solid line is a least-squares fit to the composite group data (solid points) given in Equation 14 whilst the dashed line is a least-squares fit to the field data given in Equation 15. Error bars indicate the errors on the 2MASS magnitudes and the combined errors on the colours.

tities. Therefore, the fact that the mean magnitudes in high X-ray luminosity groups are fainter than those in low X-ray luminosity groups is an indication of the higher dwarf-to-giant ratio in this environment. We suggest that the magnitude difference observed by Miles et al. (2004) is a result of the more numerous bright galaxies within $R < 0.3r_{500}$ in high-L_X groups compared to low-L_X groups (Figure 14).

10.3 Colours

Galaxy colour has been shown to depend on both luminosity and environment: The highest luminosity galaxies are the reddest (e.g. Faber 1973; Visvanathan & Sandage 1977; Balogh et al. 2004; Baldry et al. 2004; Blanton et al. 2005) and there are a higher fraction of red galaxies in the densest environments (e.g. Oemler 1974; Butcher & Oemler 1984; Girardi et al. 2003; Balogh et al. 2004; Tanaka et al. 2004). Previous analyses of the group environment have found that the colours of galaxies in groups are redder than those in the field (Girardi et al. 2003; Tovmassian et al. 2004). In order to examine the relationship between colour and environment, we separate out the effects of luminosity by correcting the colours of the galaxies to the colour they would have at a specific magnitude based on the slope of the colour-magnitude relation (c.f. Kodama et al. 2001; Tanaka et al. 2005). We therefore fit a colour-magnitude relation using the Buckley-James algorithm described above. The best-fit straight line to all 113 absolute-magnitude limited galaxies is described by:

$$B - K = -0.21^{\pm 0.03} M_K - 0.88, \quad (14)$$

with an rms scatter $\sigma = 0.49$ mag, and is shown in Figure 15. We also fit a colour-magnitude relation to the field galaxies and find that this is consistent within the errors:

$$B - K = -0.26^{\pm 0.03} M_K - 2.2. \quad (15)$$

We correct the colours of the galaxies to a magnitude of $M_K = -22$ mag based on Equation 14, i.e. $B - K_c = (B-K) - 0.21(M_K + 22)$. Examining the relationship of the normalised colours with scaled radius (Figure 16) we observe a weak correlation of colour with radius (correlated at the 86 per cent level) such that galaxies further out are bluer than those in the centre of groups. A KS test indicates that the colours of the galaxies in the high-L_X environment are unlikely to be drawn from the same parent population as those galaxies in the low-L_X groups at the 95.4 per cent level. Comparing the two group populations to the field, the colours of the galaxies in the high-L_X environment are unlikely to have been drawn from the same population as those in the field at the 99.8 per cent level. In contrast, the colours of the galaxies in the low-L_X groups are unlikely to have been drawn from the same population as the field at only the 57 per cent level. It appears that the colours of galaxies in high X-ray luminosity groups are significantly redder than those in low X-ray luminosity groups, which are similar to those of galaxies in the field.

10.4 Morphology

The morphology-density relationship, and its close equivalent the morphology-radius relationship have been known to exist in clusters for years (e.g. Dressler 1980; Whitmore et al. 1993).

In the group environment, Tran et al. (2001) and Wilman et al. (2005) have shown that the fraction of early-type galaxies in groups is higher than the field and that fraction decreases from the group core to the outer regions consistent with the situation in clusters. However, Helsdon & Ponman (2003a) find that, although groups show similar spiral fractions to clusters within a virial radius, the group morphology-density relation is offset from the cluster

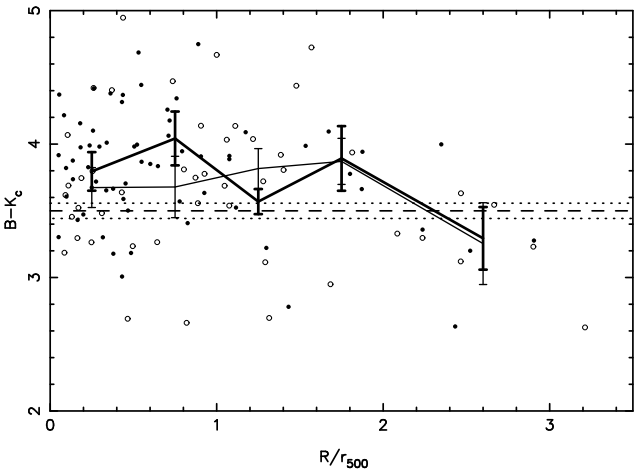

Figure 16. Relationship of $B-K$ colour with scaled group radius (R/r_{500}). The colours are normalised to $M_K = -22$ mag as described in the text. The solid points indicate galaxies in high-L_X groups ($\log_{10}L_X(r_{500}) > 41.7$ erg s^{-1}) and open points indicate galaxies in low-L_X groups ($\log_{10}L_X(r_{500}) < 41.7$ erg s^{-1}). The solid line indicates the mean colour at each radius for high-L_X groups (thick black line) and low-L_X groups (thin black line), whilst the error bars show the error on the mean colour. The dashed line indicates the mean colour of field galaxies, also normalised to $M_K = -22$ mag, whilst the dotted lines indicate the error on the mean of the field colours.

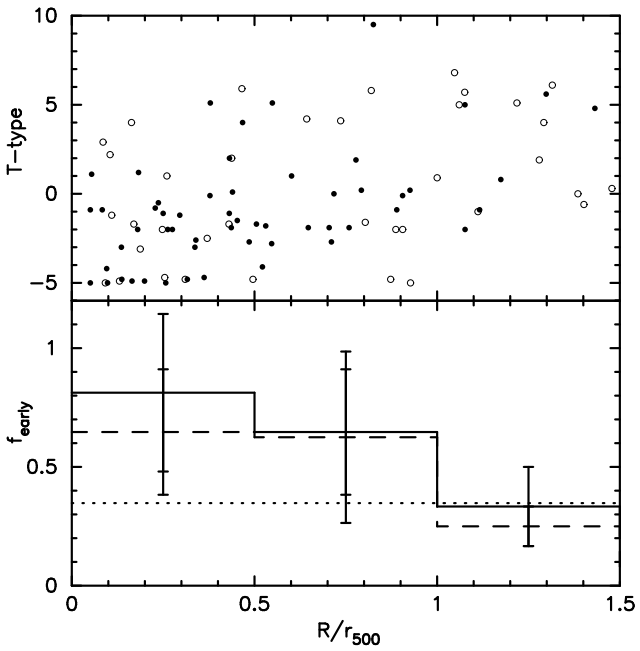

Figure 17. The upper plot indicates the morphological T-types with scaled group-radius, solid points are galaxies in high X-ray luminosity groups ($\log_{10}L_X(r_{500}) > 41.7$ erg s^{-1}), open points in low X-ray luminosity groups ($\log_{10}L_X(r_{500}) < 41.7$ erg s^{-1}). The lower plot shows the early-type fraction (f_{early}; proportion of galaxies with T-type $\leqslant 0.0$) with scaled group radius for galaxies in high-L_X groups (solid line), low-L_X groups (dashed line) and the field (dotted line). The error bars indicate poisson errors on each bin.

relation. They conclude that this is a result of the projection of the 3D density onto the line of sight and a higher merging rate in the group environment.

In Figure 17 we show the distribution of the morphologies with scaled group-centric radius. We observe that both high- and low X-ray luminosity groups have significantly higher fractions of early-type galaxies than the field value within a radius of r_{500}. These fractions become equivalent to the field at radii larger than this. A KS test confirms this, indicating that the morphologies of the galaxies in groups within r_{500} are not drawn from the same population as those in the field at the > 99.999 per cent level.

We can also compare our group early-type fractions to those in clusters if we assume that passive galaxies are equivalent to early-type galaxies. Within a radius of r_{200} ($\sim 1.5r_{500}$) Hilton et al. (2005) find a fraction of passive galaxies of 0.76 ± 0.02 in high X-ray luminosity clusters and 0.64 ± 0.02 for low-L_X clusters. For our groups we find an early-type fraction within a $1.5r_{500}$ of 0.71 ± 0.04 for high X-ray luminosity groups and 0.51 ± 0.08 for low-L_X groups, where the errors are poisson errors. There is a clear difference between the high- and low-X-ray luminosity groups and a KS test confirms that the morphologies of galaxies in high-L_X groups are not drawn from the same population as those in low-L_X groups at the 97.34 per cent level. In comparison to the clusters we find that the low-L_X groups have a lower early-type fraction than clusters and high-L_X groups have similar early-type fractions to the cluster environment. However, we bear in mind the work of Helsdon & Ponman (2003a) and add the caveat that these groups may not follow the same morphology-density relationship as clusters.

Wilman et al. (2005) observe an enhancement of the fraction of passive galaxies in group environments in comparison to the field at all magnitudes. Figure 18 demonstrates that galaxies in high X-ray luminosity groups have higher early-type fractions than the field at all magnitudes, whereas the galaxies in low X-ray luminosity groups are more consistent with the field. A KS test confirms that the morphologies of galaxies in high-L_X groups are not drawn from the same population as those in the field at > 99.999 per cent level. In contrast the galaxies in the low-L_X groups are consistent with not being drawn from the same population as those in the field at only the 58 per cent level.

In summary, groups have higher fractions of early-type galaxies than the field at radii less than r_{500} and similar fractions to the field at radii beyond this. The morphologies of galaxies in low X-ray luminosity groups are similar to those in the field whilst the morphologies of galaxies in the inner regions of high X-ray luminosity groups are similar to those in clusters.

11 DISCUSSION AND CONCLUSIONS

We have examined the properties of 16 galaxy groups from the GEMS sample (Osmond & Ponman 2004; Forbes et al. 2006) which have additional wide-field HI observations (Kilborn et al. in preparation). Using galaxy positions and recession velocities from the 6dFGS DR2, NED and new recession velocities and positions from the HI observations, we deter-

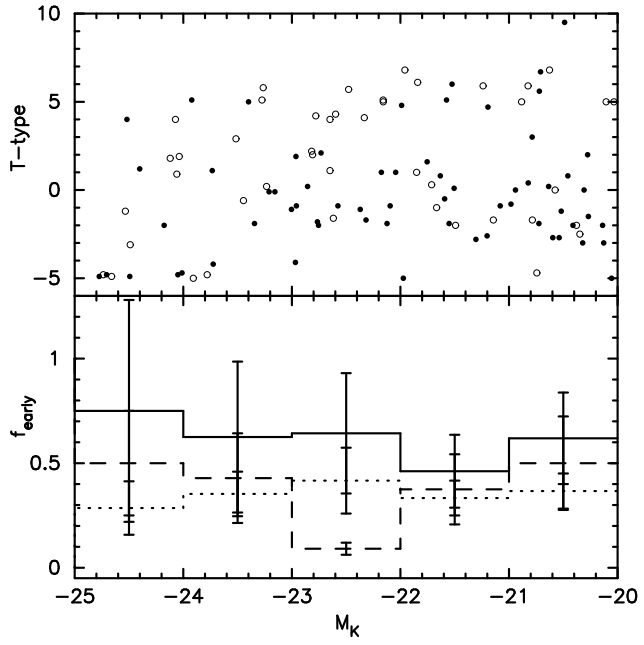

Figure 18. The upper plot shows the distribution of morphological T-types with absolute magnitude, M_K, solid points are galaxies in high X-ray luminosity groups ($\log_{10}L_X(r_{500}) >$ 41.7 erg s^{-1}), open points in low X-ray luminosity groups ($\log_{10}L_X(r_{500}) <$ 41.7 erg s^{-1}). The lower plot shows the early-type fraction (f_{early}; proportion of galaxies with T-type $\leqslant 0.0$) for galaxies in high-L_X groups (solid line), low-L_X groups (dashed line) and the field (dotted line). The error bars indicate possion errors on each bin.

mine group membership using a FOF algorithm. We show that the group properties we derive from that membership are robust to the choice of limiting number density contrast. However, we do not find a group at the position of the NGC 7144 group (determined by Osmond & Ponman 2004) at any limiting density contrast. This region only has X-ray emission from the halo of NGC 7144 itself. We, therefore, do not include this group in the rest of our analysis.

We examined the dynamical parameters of the remaining 15 groups, finding that groups with higher X-ray luminosities are more likely to show extended intra-group X-ray emission and bright early-type BGGs located near to the group centroid, than those groups with lower X-ray luminosities. Our analysis suggests that the X-ray luminosities of these groups are more closely related to their dynamical properties than whether the groups show intra-group, galaxy halo or no detectable X-ray emission as defined by Osmond & Ponman (2004).

Investigating the scaling relations followed by the galaxy groups we find that groups with higher X-ray luminosities have higher velocity dispersions and masses than those with lower X-ray luminosities: $L_X(r_{500}) \propto \sigma_v^{3.11\pm0.59}$, and $L_X(r_{500}) \propto M_V^{1.13\pm0.27}$. These relationships are consistent with the predictions of self-similarity (e.g. Borgani et al. 2004), i.e. groups following the same scaling relations as clusters. We also find the virial mass to be proportional to the total K-band luminosity in the system: $M_V \propto L_K(Tot)^{2.0\pm0.9}$, indicating that the mass of the groups is increasing faster than their luminosity. This increase in the mass-to-light ratio is unlikely to be an effect of the stellar populations of galaxies as the K-band is more closely related to galaxy mass than other wavelengths (Proctor et al. in preparation). The fraction of early-type galaxies in the groups are correlated with both velocity dispersion and X-ray luminosity.

We study the properties of the BGGs and their relationship with their host group. We find that the BGGs of the dynamically mature groups are early-type galaxies that lie close to the spatial and velocity centroid of the group. In contrast, we find both early- and late-type BGGs in the dynamically immature groups and these lie at a range of spatial and velocity separations from their group centroids. The early-type BGGs are significantly brighter than the late-type BGGs. We observe that the luminosities of all the BGGs increase with increasing total K-band luminosity, X-ray luminosity and velocity dispersion of their groups. However, the fraction of group light in the BGG, and the dominance of the BGG over the second brightest galaxy, fall with increasing total group luminosity. These properties are all consistent with the paradigm in which the group grows rapidly by accreting infalling galaxies but beyond a critical group mass the time for infalling galaxies to merge with the central galaxy is longer than a Hubble time, such that the growth of the BGG with respect to that of the group slows.

In order to analyse the properties of the groups' constituent galaxies we stack the members of the 15 groups to create a composite group. In the composite group we observe that galaxies are, in the mean, fainter, bluer and morphologically later-type galaxies with increasing radius from the group centroid. We divide the composite group sample by the X-ray luminosity ($\log_{10}L_X(r_{500}) = 41.7$ erg s^{-1}) which Miles et al. (2004) found to divide the properties of 25 GEMS groups. Galaxies in groups with an X-ray luminosity brighter than this are redder with a higher giant-to-dwarf ratio, and a higher early-type fraction (close to that observed in clusters) than galaxies in low-L_X groups. We also observe that the colours of galaxies and early-type fractions in low X-ray luminosity groups are more closely related to those of galaxies in the field, than are galaxies in high-L_X groups.

The examination of the composite group suggests that the properties of galaxies in the centres of low-mass groups are already different to those in the field, to account for the radial relationships observed. The galaxies in the centres of the groups are more likely to be bright, red, early-type galaxies than the galaxies in our field sample, even in the dynamically younger groups that do not have large velocity dispersions and are not generally observed to display halos of hot X-ray emitting gas. This suggests that multiple, high-speed galaxy-galaxy encounters ('harassment'; Moore et al. 1996) and ram pressure stripping by a dense intra-group medium (e.g. Quilis et al. 2000) cannot be playing a role in creating the observed differences in these low-mass groups.

Possible mechanisms for these differences include strangulation and merging. Strangulation stems from current theories of galaxy formation that suggest that isolated galaxies continuously draw gas from a hot diffuse reservoir in their dark matter halo with which to maintain star formation (e.g. Larson et al. 1980; Cole et al. 2000). Access to this reservoir may be halted by the galaxy falling into a group, thereby quenching its star formation. The galaxy will then

slowly fade and redden over $\sim$ 1Gyr. However, the reservoirs are too cold and diffuse to be observed (e.g. Benson et al. 2000). In contrast, galaxy mergers occur over much shorter timescales, $\sim$ 100 Myr: Once a group has formed by gravitational collapse, the system relaxes thereafter by two-body interactions, with dynamical friction causing galaxies to fall into the centre of the group and decelerate. This deceleration is proportional to the inverse of the difference in velocity between the galaxies and is therefore more likely in low-velocity dispersion groups (although there is also a dependence on the number of members a group has). Galaxy-galaxy mergers are therefore more likely in the low velocity dispersion groups.

The differences observed between field and group galaxies are stronger in higher mass groups, such that the properties of galaxies in this environment are already close to those in clusters. The dynamical analysis of all the groups suggests that the higher mass groups are more dynamically mature. We therefore conclude that the higher early-type fractions and dwarf-to-giant ratios and redder galaxies in higher mass groups are a result of galaxy-galaxy mergers at earlier epochs in smaller mass groups which have since merged to become the group we observe today, whilst, due to their lower velocity dispersions, the less massive groups are still undergoing mergers today. However, the properties of all the galaxies in the groups are unlikely to be due to mergers. We therefore conclude that strangulation, or some further mechanism may play some role and look to our second paper (Kilborn et al. in preparation) examining the neutral hydrogen in these groups to further understand the mechanisms acting in this environment.

ACKNOWLEDGMENTS

We would like to thank Chris Power, Gary Mamon, Trevor Ponman, Rob Proctor and Simon Ellis for helpful discussions. We would also like to thank the anonymous referee for his/her positive comments. This publication makes use of data products from the Two Micron All Sky Survey (2MASS) which is a joint project of the University of Massachusetts and the Infrared Processing and Analysis Center/California Institute of Technology, funded by the National Aeronautics and Space Administration and the National Science Foundation. This research has made use of the NASA/IPAC Extragalactic Database (NED) which is operated by the Jet Propulsion Laboratory, California Institute of Technology, under contract with the National Aeronautics and Space Administration. It has also made use of the HyperLEDA database.

REFERENCES

Abazajian K. et al. 2003, AJ, 126, 2081
Baldry I. K., Glazebrook K., Brinkmann J., Ivezić Ž., Lupton R. H., Nichol R. C., Szalay A. S., 2004, ApJ, 600, 681
Balogh M. L., et al., 2002, ApJ, 566, 123
Balogh M. L., Baldry I. K., Nichol R., Miller C., Bower R., Glazebrook K., 2004, ApJ, 615, 101
Barnes J., 1985, MNRAS, 215, 517
Bautz L. P., Morgan W. W., 1970, ApJ, 162, 149
Beers T. C., Flynn K., Gebhardt K., 1990, AJ, 100, 32
Benson A. J., Bower R. G., Frenk C. S., White S. D. M., 2000, MNRAS, 314, 557
Blanton M. R., Eisenstein D., Hogg D. W., Schlegel D. J., Brinkmann J., 2005, ApJ, 629, 143
Borgani S., et al., 2004, MNRAS, 348, 1078
Brough S., Collins C. A., Burke D. J., Mann R. G., Lynam P. D., 2002, MNRAS, 329, 53
Brough S., Collins C. A., Burke D. J., Lynam P. D., Mann R. G., 2005, MNRAS, 364, 1354
Brough S., Forbes D. A., Kilborn V. A., Couch W., Colless M., 2006, MNRAS, in press
Butcher H., Oemler A. Jr., 1984, ApJ, 285, 426
Carlberg R. G., Yee H. K. C., Ellingson E., 1997, ApJ, 478, 462
Carlberg R. G., Yee H. K. C., Morris S. L., Lin H., Hall P. B., Patton D. R., Sawicki M., Shepherd C. W., 2001, ApJ, 552, 427
Cellone S. A., Buzzoni A., 2005, MNRAS, 356, 41
Cole S., Lacey C. G., Baugh C. M., Frenk C. S., 2000, MNRAS, 319, 168
Cooray A., Milosavljević M., 2005, ApJ, 627, 85
Corwin H. G. Jr., de Vaucouleurs A., de Vaucouleurs G, 1977, AJ, 82, 557
Croton D. J. et al., 2005, MNRAS, 356, 1155
da Costa, L. N. et al., 1988, ApJ, 327, 544
Diaferio A., Kauffmann G., Colberg J. M., White S. D. M., 1999, MNRAS, 307, 537
Domínguez M. J., Zandivarez A. A., Martínez H. J., Merchán M. E., Muriel H., Lambas D. G., 2002, MNRAS, 335, 825
D'Onghia E., Sommer-Larsen J., Romeo A. D., Burkert A., Pedersen K., Portinari L., Rasmussen J., 2005, ApJ, 630, 109
Dressler A., 1980, ApJ, 236, 351
Edge A. C., Stewart G. C., 1991, MNRAS, 252, 428
Eke V. R. et al., 2004a, MNRAS, 348, 866
Eke V. R. et al., 2004b, MNRAS, 355, 769
Evrard A. E., Metzler C. A., Navarro J. F., 1996, ApJ, 469, 494
Faber S. M., 1973, ApJ, 179, 731
Ferguson H. C., Sandage A., 1991, AJ, 101, 765
Forbes D. A., Sánchez-Blázquez P., Phan A., Brodie J., Strader J., Spitler L., 2006, MNRAS, 366, 1230
Forbes D. A. et al. 2006, PASA, 23, 38
Garcia A. M., 1993, A&AS, 100, 47
Geller M. J., Postman M., 1983, ApJ, 274, 31
Girardi M., Manzato P., Mezzetti M., Giuricin G., Limboz F., 2002, ApJ, 569, 720
Girardi M., Mardirossian F., Marinoni C., Mezzetti M. & Rigoni E., 2003, A&A, 410, 461
Giuricin G., Marinoni C., Ceriani L., Pisani A., 2000, ApJ, 543, 178
Gómez P. L. et al., 2003, ApJ, 584, 210
Gunn J. E., Gott J R., 1972, ApJ, 176, 1
Hashimoto Y., Oemler A. Jr., 2000, ApJ, 530, 652
Heisler J., Tremaine S., Bahcall J. N, 1985, ApJ, 298, 8
Helsdon S. F., Ponman T. J., 2000, MNRAS, 315, 356
Helsdon S. F., Ponman T. J., 2003a, MNRAS, 340, 485
Helsdon S. F., Ponman T. J., 2003b, MNRAS, 339, 29
Hickson P., 1982, ApJ, 255, 382

Hilton M. et al., 2005, MNRAS, 363, 661
Huchra J. P., Geller M. J., 1982, ApJ, 257, 423
Jarrett T. H., Chester T., Cutri R., Schneider S., Skrutskie M., Huchra J. P., 2000, AJ, 119, 2498
Jensen J. B. et al., 2003, ApJ, 583, 712
Jones L. R., Ponman T. J., Horton A., Babul A., Ebeling H., Burke D. J., 2003, MNRAS, 343, 627
Jones D. H. et al., 2004, MNRAS, 355, 747
Jones D. H., Saunders W., Read M., Colless M., 2005, PASA, 22, 277
Kilborn V. A., Koribalski B. S., Forbes D. A., Barnes D. G., Musgrave R. C., 2005, MNRAS, 356, 77
Kilborn V. A. et al., 2006, MNRAS, submitted
Klemola A. R., 1969, AJ, 74, 804
Kochanek C. S. et al., 2001, ApJ, 560, 566
Kodama, T., Smail, I., Nakata, F., Okamura, S., Bower, R. G. 2001, ApJL, 562, 9
Larson R. B., Tinsley B. M., Caldwell C. N., 1980, ApJ, 237, 692
Lazzati D., Chincarini G., 1998, A&A, 339, 52
Lewis I. et al., 2002, MNRAS, 334, 673
Lin Y-T, Mohr J. J., 2004, ApJ, 617, 879
Loh Y.-S., Strauss M. A., 2006, MNRAS, 366, 373
Łokas E. L., Mamon G. A., 2003, MNRAS, 343, 401
Longo G., Busarello G., Lorenz H., Richter G., Zaggia S. 1994, A&A, 282, 418
Mahdavi A., Geller M. J., 2001, ApJ, 554, 129
Maia M. A. G., da Costa L. N., Latham D. W., 1989, ApJS, 69, 809
Mamon G. A., 1993, astro-ph/9308032
Marinoni C., Monaco P., Giuricin G., Costantini B., 1998, ApJ, 505, 484
Marinoni C., Hudson M. J., 2002, ApJ, 569, 101
Miles T. A., Raychaudhury S., Forbes D. A., Goudfrooij P., Ponman T. J., Kozhurina-Platais V., 2004, MNRAS, 355, 785
Moore B., Katz N., Lake G., Dressler A., Oemler A., 1996, Nature, 379, 613
Mulchaey J. S., Zabludoff A. I., 1998, ApJ, 496, 73
Nolthenius R., White S. D. M., 1987, MNRAS, 225, 505
Nolthenius R., Klypin A. A., Primack J. R., 1997, ApJ, 480, 43
Oegerle W. R., Hill J. M., 2001, AJ, 122, 2858
Oemler A. Jr., 1974, ApJ, 194, 1
Oemler A. Jr., 1992, Clusters and Superclusters of Galaxies conference proceedings, Kluwer, 29
Osmond J. P. F., Ponman T. J., 2004, MNRAS, 350, 1511
O'Sullivan E., Forbes D. A., Ponman T. J., 2001, MNRAS, 328, 461
Parker L. C., Hudson M. J., Carlberg R. G., Hoekstra H., ApJ, 634, 806
Paturel G. et al., 1997, A&AS, 124, 109
Ponman T. J., Bourner P. D. J., Ebeling H., Bohringer H., 1996, MNRAS, 283, 690
Quilis V., Moore B., Bower R., 2000, Science, 288, 1617
Quintana H., Melnick J., 1982, AJ, 87, 972
Ramella M., Geller M. J., Huchra J. P., Thorstensen J. R., 1995, AJ, 109, 1458
Ramella M., Boschin W., Geller M. J., Mahdavi A., Rines K., 2004, AJ, 128, 2022
Sanderson A. J. R., Ponman T., 2003, MNRAS, 345, 1241
Schechter P., 1976, ApJ, 203, 297
Schlegel D. J., Finkbeiner D. P., Davis M., 1998, ApJ, 500, 525
Tanaka M., Goto T., Okamura S., Shimasaku K., Brinkmann J., 2004, AJ, 128, 2677
Tanaka M. et al., 2005, MNRAS, 362, 268
Tonry J. L. et al., 2001, ApJ, 546, 681
Tovmassian H. M., Plionis M., Andernach H., 2004, ApJ, 617, 111
Tran K-V. H., Simard L., Zabludoff A. I., Mulchaey J. S., 2001, ApJ, 549, 172
Trentham N., Tully R. B.,Mahdavi A., 2006, MNRAS, in press
Tully R. B., 1980, ApJ, 237, 390
Tully R. B., 1987, ApJ, 321, 280
van den Bosch F. C., Weinmann S. M., Yang X., Mo H. J., Li C., Jing Y. P., 2005, MNRAS, 361, 1203
Visvanathan N., Sandage A, 1977, ApJ, 216, 214
Wake D. A., Collins C. A., Nichol R. C., Jones L. R., Burke D. J., 2005, ApJ, 627, 186
Wilman D. J. et al., 2005, MNRAS, 358, 71
Whitmore B. C., Gilmore D. M., Jones C., 1993, ApJ, 407, 489
Zabludoff A. I., Mulchaey J. S., 2000, ApJ, 539, 136
Zabludoff A. I., Mulchaey J. S., 1998, ApJ, 496, 39
Zabludoff A. I., Huchra J. P., Geller M. J., 1990, ApJS, 74, 1
Zaritsky D., Zabludoff A. I., Gonzalez A. H., 2006, ApJ, 638, 725

APPENDIX A: GROUP MEMBERS

APPENDIX B: SPATIAL DISTRIBUTION OF GROUPS

This paper has been typeset from a TEX/ LATEX file prepared by the author.

Table A1. Details of the galaxies in each group. R_{gc} is the group-centric radius of each galaxy from the centre calculated by the FOF algorithm. New galaxies found in HI are named GEMS-groupname-number. Dashes indicate where information is not available.

Galaxy Name	6dFGS ID	RA (J2000)	Dec (J2000)	$\bar{v}$ (km s^{-1})	m_K (mag)	R_{gc} (Mpc)	T-type
NGC 524							
UGC 00896	-	1:21:27.40	9:10:47.30	2042	13.50±0.111	0.325	8.0
NGC 0489	-	1:21:53.90	9:12:23.60	2507	9.61±0.179	0.281	5.0
CGCG 411-038	-	1:22:31.82	9:16:53.20	2636	13.43±0.287	0.213	0.0
MCG +01-04-042	-	1:22:54.30	8:51:17.00	2219	13.50±0.184	0.297	0.0
NGC 0502	-	1:22:55.54	9: 2:57.10	2489	10.28±0.069	0.235	-2.0
NGC 0509	-	1:23:24.09	9:26: 0.80	2274	10.99±0.410	0.114	-1.7
NGC 0516	-	1:24: 8.07	9:33: 6.10	2432	10.63±0.410	0.045	-1.7
IC 0101	-	1:24: 8.55	9:55:49.90	2404	12.13±0.132	0.173	3.0
NGC 0518	-	1:24:17.64	9:19:51.40	2725	9.92±0.113	0.069	1.0
NGC 0522	-	1:24:45.85	9:59:40.70	2725	9.44±0.086	0.195	4.1
NGC 0524	-	1:24:47.72	9:32:19.80	2379	7.24±0.218	0.029	-1.2
NGC 0532	-	1:25:17.34	9:15:50.80	2361	8.96±0.367	0.116	2.0
IC 0114	-	1:26:22.58	9:54:35.80	2275	11.39±0.108	0.240	-2.0
UGC 01019	-	1:26:38.94	10:17:14.00	2182	13.50±0.100	0.369	8.9
LEDA 093841	-	1:27:37.30	8:50:24.00	2435	13.50±0.100	0.394	0.0
UGC 01050	-	1:28:12.80	10:26: 2.00	2396	13.50±0.001	0.510	8.0
NGC 720							
KUG 0150-138	-	1:52:36.06	-13:34:39.70	1374	13.50±0.225	0.106	0.0
2MASX J01524752-1416211	6dF J0152475-141621	1:52:47.53	-14:16:21.40	1448	11.48±0.328	0.223	0.0
NGC 0720	6dF J0153005-134419	1:53: 0.49	-13:44:19.00	1663	7.40±0.401	0.021	-4.9
2MASX J01535632-1350125	-	1:53:56.32	-13:50:12.60	1496	12.40±0.217	0.100	0.0
MCG -02-05-072	-	1:54: 3.15	-14:15:10.70	1423	10.34±0.555	0.238	0.3
6dF J0154050-135421	6dF J0154050-135421	1:54: 5.04	-13:54:21.20	1321	13.50±0.100	0.126	99.9
NGC 1052							
[RC3] 0231.5-0635	-	2:33:57.04	-6:21:36.20	1410	13.50±0.100	0.766	99.9
USGC S092 NED09	-	2:35:28.79	-7: 8:59.00	1532	13.50±0.100	0.535	99.9
6dF J0235320-070936	6dF J0235320-070936	2:35:32.00	-7: 9:36.30	1554	13.50±0.100	0.530	99.9
NGC 0991	-	2:35:32.69	-7: 9:16.00	1532	11.18±0.361	0.530	5.0
NGC 1022	-	2:38:32.70	-6:40:38.70	1453	8.64±0.367	0.440	1.1
SDSS J023848.50-080257.7	-	2:38:48.50	-8: 2:57.70	1665	13.50±0.100	0.240	99.9
NGC 1035	-	2:39:29.09	-8: 7:58.60	1241	9.13±0.465	0.201	5.1
6dF J0239299-080821	6dF J0239299-080821	2:39:29.92	-8: 8:21.10	1393	13.50±0.100	0.201	99.9
NGC 1042	6dF J0240240-082601	2:40:23.97	-8:26: 1.00	1411	9.45±0.576	0.217	6.1
UGCA 038	-	2:40:30.19	-6: 6:23.00	1327	13.50±0.100	0.549	9.0
NGC 1047	-	2:40:32.84	-8: 8:51.60	1340	11.38±0.173	0.137	-0.7
NGC 0961	-	2:41: 2.46	-6:56: 9.10	1295	13.50±0.100	0.286	99.9
NGC 1052	6dF J0241048-081521	2:41: 4.80	-8:15:21.00	1591	7.51±0.360	0.144	-4.8
SDSS J024120.22-071706.0	-	2:41:20.22	-7:17: 6.00	1663	13.50±0.100	0.173	99.9
[VC94] 023858-0820.4	-	2:41:25.53	-8: 7:36.70	1412	13.50±0.100	0.097	99.9
SDSS J024129.37-072046.0	-	2:41:29.37	-7:20:46.00	1145	13.50±0.100	0.153	99.9
2MASX J02413514-0810243	6dF J0241351-081025	2:41:35.11	-8:10:24.60	1556	13.15±0.100	0.109	0.0
SDSS J024149.95-075530.1	-	2:41:49.96	-7:55:30.00	1372	13.50±0.100	0.031	99.9
SDSS J024246.84-073230.3	-	2:42:46.84	-7:32:30.40	1344	13.50±0.100	0.122	99.9
MCG -01-08-001	-	2:43:42.80	-6:39: 5.00	1410	13.50±0.100	0.401	9.8
NGC 1084	-	2:45:59.93	-7:34:43.10	1407	8.01±0.665	0.344	5.1
SHOC 137	6dF J0248158-081724	2:48:15.83	-8:17:23.90	1405	13.50±0.100	0.533	99.9
SDSS J024839.95-074848.3	-	2:48:39.96	-7:48:48.30	1465	13.50±0.100	0.545	99.9
SHOC 138a	-	2:49: 9.32	-7:50:27.40	1288	13.50±0.100	0.583	99.9
NGC 1110	-	2:49: 9.57	-7:50:15.20	1333	13.50±0.273	0.583	8.8
SHOC 138b	-	2:49:10.79	-7:49:24.50	1368	13.50±0.100	0.585	99.9
SDSS J024911.16-082828.7	-	2:49:11.16	-8:28:28.80	1430	13.50±0.100	0.620	99.9
SDSS J024913.41-080653.2	-	2:49:13.42	-8: 6:53.20	1369	13.50±0.100	0.595	99.9
2MASX J02400428-0744217	6dF J0240043-074422	2:40: 4.28	-7:44:22.00	1309	13.09±0.100	0.133	0.0

Table A2. Continued.

Galaxy Name	6dFGS ID	RA (J2000)	Dec (J2000)	$\bar{v}$ (km s^{-1})	m_K (mag)	R_{gc} (Mpc)	T-type
NGC 1332							
NGC 1315	6dF J0323066-212231	3:23: 6.60	-21:22:30.70	1596	9.94±0.474	0.249	-1.0
NGC 1325	6dF J0324256-213238	3:24:25.57	-21:32:38.30	1589	8.83±0.169	0.144	4.2
NGC 1325A	-	3:24:48.50	-21:20:10.00	1333	14.03±0.517	0.095	6.6
ESO 548- G 011	-	3:24:55.30	-21:47: 2.00	1453	13.50±0.104	0.173	8.4
2MASX J03255262-2117204	6dF J0325526-211721	3:25:52.62	-21:17:20.60	1427	11.77±0.100	0.029	0.0
NGC 1332	-	3:26:17.32	-21:20: 7.30	1524	7.12±0.368	0.042	-3.1
NGC 1331	6dF J0326283-212120	3:26:28.34	-21:21:20.30	1241	10.87±0.202	0.057	-4.7
2MASX J03263135-2113003	-	3:26:31.31	-21:13: 0.60	1548	11.26±0.091	0.083	-2.5
2MASX J03273556-2113417	6dF J0327356-211341	3:27:35.57	-21:13:41.40	1744	12.12±0.100	0.167	99.9
6dF J0327422-214159	6dF J0327422-214159	3:27:42.16	-21:41:58.60	1294	13.50±0.100	0.208	99.9
NGC 1407							
NGC 1383	6dF J0337392-182022	3:37:39.24	-18:20:22.10	2008	9.51±0.427	0.336	-1.9
NGC 1390	-	3:37:52.17	-19: 0:30.10	1207	11.70±0.209	0.350	1.2
NGC 1393	-	3:38:38.58	-18:25:40.70	2127	9.31±0.475	0.241	-1.7
ESO 548- G 063	6dF J0339348-200053	3:39:34.78	-20: 0:53.30	2047	12.18±0.162	0.555	3.7
ESO 548- G 064	6dF J0340001-192535	3:40: 0.08	-19:25:34.70	1873	11.03±0.212	0.339	-2.7
ESO 548- G 065	-	3:40: 2.70	-19:21:59.80	1221	13.21±0.138	0.317	1.3
IC 0343	-	3:40: 7.14	-18:26:36.50	1841	10.65±0.262	0.109	-0.8
NGC 1407	-	3:40:11.90	-18:34:49.40	1779	6.86±0.453	0.095	-4.9
2MASX J03401592-1904544	6dF J0340159-190454	3:40:15.93	-19: 4:54.40	1613	12.26±0.297	0.213	-3.5
ESO 548- G 068	-	3:40:19.17	-18:55:53.40	1693	10.43±0.225	0.162	-2.6
2MASX J03404323-1838431	6dF J0340432-183843	3:40:43.23	-18:38:43.10	1373	12.36±0.170	0.059	-1.6
2MASX J03405272-1828410	6dF J0340527-182841	3:40:52.73	-18:28:40.80	1678	12.70±0.084	0.042	-1.4
ESO 548- G 072	-	3:41: 0.28	-19:27:19.40	2034	13.50±0.124	0.331	5.0
ESO 548- G 073	6dF J0341044-190540	3:41: 4.41	-19: 5:40.00	989	12.91±0.212	0.199	3.3
IC 0345	6dF J0341091-181851	3:41: 9.13	-18:18:50.90	1244	11.22±0.249	0.086	-2.0
ESO 548- G 076	6dF J0341318-195419	3:41:31.81	-19:54:18.50	1544	11.88±0.362	0.495	-1.3
IC 0346	-	3:41:44.66	-18:16: 1.10	2013	10.04±0.533	0.113	-0.5
6dF J0341498-193453	6dF J0341498-193453	3:41:49.82	-19:34:52.50	1913	13.50±0.100	0.380	99.9
ESO 548- G 079	6dF J0341561-185343	3:41:56.08	-18:53:42.60	2029	11.11±0.445	0.141	-1.2
ESO 549- G 002	-	3:42:57.34	-19: 1:12.40	1111	13.50±0.323	0.232	9.5
APMBGC 549+118-079	-	3:44: 2.46	-18:28:18.30	1979	13.50±0.100	0.257	99.9
ESO 549- G 007	6dF J0344115-191910	3:44:11.48	-19:19: 9.90	1478	13.50±0.121	0.389	-1.4
NGC 1440	-	3:45: 2.91	-18:15:57.70	1597	8.28±0.699	0.362	-1.9
NGC 1452	-	3:45:22.31	-18:38: 1.10	1737	8.77±0.206	0.378	0.2
NGC 1566							
NGC 1546	6dF J0414364-560340	4:14:36.38	-56: 3:39.51	1238	8.17±0.592	0.164	-0.6
NGC 1549	6dF J0415451-553532	4:15:45.13	-55:35:32.10	1202	6.88±0.113	0.058	-4.8
NGC 1553	6dF J0416105-554648	4:16:10.47	-55:46:48.00	1172	6.35±0.218	0.029	-2.0
IC 2058	-	4:17:54.35	-55:55:58.40	1379	10.99±0.240	0.197	6.8
NGC 1808							
NGC 1792	6dF J0505144-375851	5: 5:14.41	-37:58:50.50	1176	7.09±0.170	0.025	4.0
2MASX J05061389-3803154	6dF J0506139-380316	5: 6:13.89	-38: 3:15.60	855	11.72±0.382	0.065	0.0
NGC 1808:[AB70] C	6dF J0507423-373046	5: 7:42.34	-37:30:46.10	969	13.50±0.100	0.205	99.9
ESO 305- G 009	-	5: 8: 7.62	-38:18:33.51	1021	13.50±0.902	0.225	8.0
2MASX J05081153-3657351	6dF J0508115-365735	5: 8:11.51	-36:57:35.30	1073	12.92±0.100	0.350	0.0
NGC 1827	6dF J0510046-365737	5:10: 4.11	-36:57:34.90	1037	10.34±0.336	0.444	5.9

Table A3. Continued.

Galaxy Name	6dFGS ID	RA (J2000)	Dec (J2000)	$\bar{v}$ (km s^{-1})	m_K (mag)	R_{gc} (Mpc)	T-type
NGC 3557							
ESO 377- G 012	6dF J1108198-373726	11: 8:19.76	-37:37:26.10	3486	10.22±0.398	0.322	1.9
NGC 3557:[ZM2000] 0038	-	11: 8:50.20	-37:22:39.00	3062	13.50±0.100	0.239	99.9
NGC 3557:[ZM2000] 0097	-	11: 9: 6.50	-37:13: 4.00	2751	13.50±0.100	0.275	99.9
NGC 3557:[ZM2000] 0047	-	11: 9: 8.40	-37:43:32.00	3146	13.50±0.100	0.225	99.9
NGC 3557:[ZM2000] 0016	-	11: 9:10.80	-37:23:59.00	3183	13.50±0.100	0.175	99.9
NGC 3557:[ZM2000] 0025	-	11: 9:21.80	-37:27:48.00	2772	13.50±0.100	0.125	99.9
NGC 3557:[ZM2000] 0049	-	11: 9:27.70	-37:38:43.00	2640	13.50±0.100	0.141	99.9
NGC 3557B	6dF J1109321-372059	11: 9:32.13	-37:20:58.70	2937	9.17±0.551	0.150	-4.7
2MASX J11093481-3737266	6dF J1109355-373729	11: 9:35.57	-37:37:28.90	2902	13.55±0.100	0.113	99.9
NGC 3557	6dF J1109577-373221	11: 9:57.65	-37:32:21.00	3031	7.28±0.121	0.021	-5.0
NGC 3557:[ZM2000] 0017	-	11:10:13.60	-37:24:55.01	2447	13.50±0.100	0.084	99.9
NGC 3564	6dF J1110364-373251	11:10:36.38	-37:32:51.30	2779	9.00±0.101	0.114	-2.0
NGC 3568	6dF J1110486-372652	11:10:48.57	-37:26:52.30	2440	9.26±0.585	0.157	5.1
NGC 3557:[ZM2000] 0032	-	11:11:42.70	-37:32:10.00	2623	13.50±0.100	0.317	99.9
NGC 3783							
ESO 320- G 004	6dF J1134436-381503	11:34:43.62	-38:15: 3.20	2829	11.94±0.200	0.397	5.0
2MASX J11351493-3755309	6dF J1135149-375531	11:35:14.92	-37:55:30.70	2823	13.15±0.100	0.250	0.0
NGC 3742	6dF J1135325-375723	11:35:32.51	-37:57:23.01	2715	8.79±0.175	0.206	1.9
AM 1133-374	-	11:35:45.70	-38: 1:19.99	2870	13.50±0.100	0.185	99.9
NGC 3749	6dF J1135532-375951	11:35:53.21	-37:59:50.50	2742	8.77±0.191	0.161	0.9
ESO 320- G 013	6dF J1137199-380551	11:37:19.86	-38: 5:51.21	3018	13.50±0.118	0.145	3.0
6dF J1138589-380042	6dF J1138589-380042	11:38:58.91	-38: 0:41.90	2685	13.50±0.100	0.344	99.9
NGC 3783	6dF J1139017-374419	11:39: 1.72	-37:44:18.90	2817	8.71±0.316	0.360	1.8
GEMS N3783-8		11:38: 1.80	-37:57: 0.10	2983	13.50±0.100	0.190	99.9
NGC 3923							
ESO 440- G 004	-	11:45:41.88	-28:21:59.50	1842	13.50±0.090	0.445	8.0
ESO 504- G 014	-	11:46:23.53	-27:15: 4.30	1645	13.50±0.106	0.638	0.0
NGC 3885	6dF J1146465-275520	11:46:46.49	-27:55:19.80	2094	8.44±0.983	0.430	0.2
6dF J1146465-280737	6dF J1146465-280737	11:46:46.50	-28: 7:37.20	2157	13.50±0.100	0.386	99.9
6dF J1147555-281157	6dF J1147555-281157	11:47:55.51	-28:11:56.70	1414	13.50±0.100	0.282	99.9
6dF J1148198-290400	6dF J1148198-290400	11:48:19.82	-29: 4: 0.30	1894	13.50±0.100	0.242	99.9
UGCA 247	6dF J1148456-281734	11:48:45.62	-28:17:34.90	1978	13.50±0.340	0.200	6.8
ESO 504- G 017	6dF J1148464-272245	11:48:46.31	-27:22:45.00	1874	11.64±0.512	0.497	5.0
ESO 440- G 012	6dF J1148584-282641	11:48:58.42	-28:26:40.50	1540	13.50±0.351	0.150	0.0
NGC 3904	6dF J1149132-291636	11:49:13.23	-29:16:36.90	1685	7.76±0.353	0.254	-5.0
ESO 440- G 014	6dF J1150032-284017	11:50: 3.20	-28:40:17.10	1888	13.50±0.179	0.028	0.0
ESO 440- G 015	6dF J1150117-283041	11:50:11.70	-28:30:41.20	1865	12.57±0.394	0.055	0.2
ESO 440- G 016	6dF J1150198-283231	11:50:19.84	-28:32:31.30	2158	12.07±0.344	0.042	-2.0
2MASX J11503040-2852202	6dF J1150304-285220	11:50:30.40	-28:52:20.30	1661	11.76±0.100	0.082	-5.0
NGC 3923	6dF J1151017-284821	11:51: 1.74	-28:48:21.20	1808	6.64±0.117	0.085	-4.8
6dF J1151122-271459	6dF J1151122-271459	11:51:12.15	-27:14:59.20	1675	13.50±0.100	0.529	99.9
2MASX J11513759-2847291	6dF J1151376-284729	11:51:37.61	-28:47:29.10	1841	12.97±0.328	0.129	-5.0
6dF J1151533-281047	6dF J1151533-281047	11:51:53.27	-28:10:46.80	1423	13.50±0.100	0.228	99.9
2MASX J11521217-2912554	6dF J1152122-291256	11:52:12.19	-29:12:55.80	1823	13.72±0.100	0.270	0.0
NGC 3936	6dF J1152206-265421	11:52:20.59	-26:54:21.20	2011	9.07±0.193	0.676	4.3
ESO 440- G 023	6dF J1152334-290719	11:52:33.40	-29: 7:19.40	1912	13.50±0.260	0.269	3.0
UGCA 250	6dF J1153241-283311	11:53:24.06	-28:33:11.40	1700	9.71±0.088	0.287	6.8
2MASX J11532725-2833064	6dF J1153273-283306	11:53:27.25	-28:33: 6.00	1664	12.20±0.100	0.291	99.9
ESO 504- G 024	-	11:53:37.89	-26:59:44.90	1894	13.50±0.123	0.688	8.9
ESO 504- G 025	-	11:53:50.64	-27:21: 0.00	1637	13.50±0.797	0.584	8.7
ESO 504- G 028	6dF J1154544-271505	11:54:54.41	-27:15: 4.70	2077	11.95±0.173	0.672	6.9
ESO 440- G 030	-	11:55:25.58	-28:44: 8.30	1821	13.50±0.267	0.473	3.0
FLASH J115712.00-280934.8	-	11:57:12.00	-28: 9:34.80	1837	13.50±0.100	0.663	99.9
ESO 504- G 030	6dF J1157149-274200	11:57:14.90	-27:42: 0.30	1841	13.50±0.115	0.733	7.6
[KK2000] 47	-	11:57:30.77	-28: 7:27.20	2125	13.50±0.100	0.695	99.9

Table A4. Continued.

Galaxy Name	6dFGS ID	RA (J2000)	Dec (J2000)	$\bar{v}$ (km s^{-1})	m_K (mag)	R_{gc} (Mpc)	T-type
NGC 4636							
NGC 4544	-	12:35:36.60	3: 2: 4.30	1154	10.22±0.065	0.460	0.8
NGC 4580	-	12:37:48.39	5:22: 6.70	1034	8.92±0.218	0.646	1.6
NGC 4586	-	12:38:28.40	4:19: 8.70	794	8.63±0.107	0.422	1.0
NGC 4587	-	12:38:35.44	2:39:26.70	901	10.54±0.080	0.296	-2.0
NGC 4600	-	12:40:22.99	3: 7: 3.80	852	9.95±0.220	0.178	-1.9
VCC 1920	-	12:42:21.25	2: 3:59.30	1311	12.94±0.854	0.236	-2.0
NGC 4630	-	12:42:31.16	3:57:37.10	737	10.19±0.224	0.227	9.5
NGC 4636	-	12:42:49.87	2:41:16.00	938	6.63±0.196	0.087	-4.8
VCC 1947	-	12:42:56.32	3:40:35.30	974	11.19±0.355	0.156	-5.0
NGC 4643	-	12:43:20.14	1:58:42.10	1273	7.47±0.189	0.249	-0.1
NGC 4665	-	12:45: 5.97	3: 3:20.60	785	7.52±0.325	0.104	-0.1
NGC 4688	-	12:47:46.46	4:20: 9.90	986	11.67±0.638	0.406	6.0
CGCG 043-030	-	12:47:59.82	4:41:41.30	1023	12.99±0.870	0.482	0.0
NGC 4701	-	12:49:11.57	3:23:19.40	723	9.96±0.244	0.357	5.6
NGC 4713	-	12:49:57.87	5:18:41.10	652	9.97±0.288	0.669	6.7
NGC 4765	-	12:53:14.42	4:27:47.20	716	10.94±0.146	0.678	0.2
NGC 4808	-	12:55:48.95	4:18:14.80	778	9.15±0.086	0.799	6.0
NGC 5044							
2MASX J13115849-1644541	6dF J1311585-164454	13:11:58.49	-16:44:54.10	2907	12.03±0.569	0.396	0.0
NGC 5010	-	13:12:26.35	-15:47:52.30	2975	9.38±0.354	0.491	-0.9
MCG -03-34-014	-	13:12:35.43	-17:32:32.70	2760	8.94±0.101	0.594	5.0
NGC 5017	6dF J1312545-164557	13:12:54.50	-16:45:57.00	2451	9.37±0.166	0.288	-4.1
MCG -03-34-019	6dF J1313055-162841	13:13: 5.48	-16:28:41.30	1989	10.79±0.658	0.241	-1.9
MCG -03-34-020	-	13:13:12.48	-16: 7:50.10	2663	11.03±0.594	0.302	-2.8
LEDA 083798	-	13:13:28.42	-16:18:52.90	2682	13.50±0.134	0.220	7.0
MCG -03-34-022	-	13:13:32.24	-17: 4:43.40	2929	10.16±0.200	0.332	1.0
6dF J1313501-173048	6dF J1313501-173048	13:13:50.08	-17:30:47.80	2223	13.50±0.100	0.518	99.9
NGC 5030	-	13:13:54.15	-16:29:27.40	2535	9.97±0.174	0.138	-1.1
2MASX J13135622-1616244	6dF J1313562-161624	13:13:56.23	-16:16:24.40	2445	12.21±0.116	0.186	-3.0
2MASXi J1313594-162303	-	13:13:59.52	-16:23: 3.80	2411	13.50±0.100	0.145	99.9
NGC 5031	-	13:14: 3.22	-16: 7:23.20	2839	9.33±0.095	0.238	-1.1
LEDA 083813	-	13:14: 7.40	-16:25:35.80	2661	13.50±0.121	0.121	-5.0
2MASX J13141733-1626189	-	13:14:17.36	-16:26:19.50	2462	12.51±0.121	0.099	-5.0
MCG -03-34-025	6dF J1314304-173201	13:14:30.42	-17:32: 0.90	2517	11.70±0.100	0.511	0.2
2MASX J13143485-1629289	6dF J1314349-162929	13:14:34.86	-16:29:28.90	2397	12.28±0.109	0.054	-5.0
NGC 5035	-	13:14:49.23	-16:29:33.70	2181	9.76±0.431	0.028	-0.9
NGC 5037	-	13:14:59.37	-16:35:25.10	1887	8.60±0.262	0.030	1.1
NGC 5038	-	13:15: 2.13	-15:57: 6.50	2222	9.57±0.247	0.293	-1.8
2MASX J13150409-1623391	6dF J1315041-162339	13:15: 4.08	-16:23:39.30	1977	12.67±0.496	0.070	-5.0
MCG -03-34-033	-	13:15:17.57	-16:29:10.20	3442	11.26±0.627	0.046	-0.9
NGC 5044	-	13:15:23.97	-16:23: 7.90	2704	7.84±0.394	0.091	-4.9
2MASX J13153203-1628509	6dF J1315320-162851	13:15:32.04	-16:28:51.10	3249	12.02±0.107	0.075	-3.0
NGC 5046	-	13:15:45.12	-16:19:36.60	2214	10.36±0.216	0.142	-5.0
NGC 5049	-	13:15:59.30	-16:23:49.80	2744	9.58±0.574	0.145	-2.0
2MASX J13164875-1620397	6dF J1316488-162040	13:16:48.75	-16:20:39.70	2619	12.07±0.130	0.250	-1.5
MCG -03-34-040	6dF J1316562-163535	13:16:56.23	-16:35:34.70	2112	12.90±0.108	0.250	7.8
NGC 5054	-	13:16:58.49	-16:38: 5.50	1741	7.82±0.556	0.258	4.0
MCG -03-34-041	-	13:17: 6.13	-16:15: 7.90	2628	10.76±1.477	0.303	5.1
LCSB S1851O	6dF J1317364-163225	13:17:36.37	-16:32:25.30	2919	12.17±0.100	0.332	99.9
GEMS N5044-1		13:14: 9.93	-16:41:41.60	3074	13.50±0.100	0.132	99.9

Table A5. Continued.

Galaxy Name	6dFGS ID	RA (J2000)	Dec (J2000)	$\bar{v}$ (km s^{-1})	m_K (mag)	R_{gc} (Mpc)	T-type
HCG 90							
ESO 466- G 025	6dF J2158245-321411	21:58:24.45	-32:14:11.50	2497	12.00±0.271	0.608	3.0
2dFGRS S407Z170	-	21:59: 0.59	-31:45: 3.20	2492	13.50±0.170	0.498	0.0
ESO 466- G 029	-	21:59:15.46	-31:13:42.70	2772	13.50±0.200	0.630	0.0
2dFGRS S407Z162	-	21:59:15.50	-31:13:18.60	2832	13.50±0.100	0.633	0.0
NGC 7163	6dF J2159204-315259	21:59:20.45	-31:52:59.30	2737	10.06±0.483	0.434	2.1
MCG -05-52-001	-	21:59:56.62	-31:27:42.60	2540	11.85±0.224	0.451	0.0
ESO 404- G 018	-	22: 1:10.16	-32:34:43.69	2268	13.50±0.252	0.428	6.7
ESO 466- G 036	-	22: 1:20.46	-31:31:46.90	2559	11.16±0.831	0.283	0.8
2dFGRS S408Z202	-	22: 1:21.44	-31:31:52.90	2457	13.50±0.100	0.281	99.9
DUKST 466-064	-	22: 1:29.79	-31:57:46.90	2760	13.50±0.175	0.095	0.0
NGC 7172	6dF J2202019-315211	22: 2: 1.87	-31:52:11.10	2557	8.39±0.172	0.044	1.2
NGC 7173	-	22: 2: 3.19	-31:58:25.30	2497	9.07±0.516	0.023	-4.2
2dFGRS S407Z097	-	22: 2: 4.81	-31:52:13.50	2384	13.50±0.100	0.043	0.0
[PCM2000] 31	-	22: 2: 5.33	-31:58:56.50	2674	13.50±0.100	0.028	99.9
NGC 7174	6dF J2202065-315934	22: 2: 6.49	-31:59:33.90	2746	13.50±0.826	0.034	2.5
IRAS 21592-3214	-	22: 2: 7.50	-31:59:28.00	2778	13.50±0.826	0.034	2.5
NGC 7176	6dF J2202085-315923	22: 2: 8.45	-31:59:23.30	2503	8.09±0.177	0.033	-4.8
ESO 466- G 043	-	22: 2:14.95	-31:13:12.40	2608	11.60±0.375	0.452	4.7
ESO 466- G 044	-	22: 2:15.88	-31:45:23.30	2818	12.25±0.173	0.117	-2.7
2dFGRS S408Z175	-	22: 2:15.89	-31:13: 6.10	2679	13.50±0.100	0.453	99.9
2dFGRS S407Z090	-	22: 2:16.07	-31:57:11.80	2541	13.50±0.180	0.029	0.0
ESO 466- G 046	6dF J2202440-315926	22: 2:44.01	-31:59:26.20	2260	11.28±0.204	0.106	0.1
NGC 7187	6dF J2202445-324811	22: 2:44.49	-32:48:11.60	2740	13.50±0.425	0.553	-1.0
ESO 466- G 047	-	22: 2:46.05	-31:57:19.70	2556	13.50±0.137	0.107	5.0
DUKST 404-032	6dF J2202502-323437	22: 2:50.17	-32:34:36.80	2221	13.50±0.150	0.418	0.0
2dFGRS S408Z047	-	22: 3:36.51	-32:26:54.19	2649	13.50±0.118	0.399	0.0
2dFGRS S408Z045	-	22: 3:41.65	-32:44:44.40	2871	13.50±0.236	0.566	0.0
ESO 404- G 027	6dF J2203478-321706	22: 3:47.84	-32:17: 6.00	2611	10.80±0.247	0.345	4.8
ESO 466- G 051	6dF J2203484-315721	22: 3:48.36	-31:57:20.90	2674	10.70±0.254	0.269	-0.9
ESO 404- G 028	6dF J2204152-323615	22: 4:15.23	-32:36:14.80	2377	11.97±0.324	0.539	0.4
2dFGRS S408Z018	-	22: 5:13.33	-32:22:32.80	2800	13.50±0.100	0.563	0.0
2dFGRS S409Z039	-	22: 5:21.08	-31:59:59.70	2401	13.50±0.305	0.513	2.5
2dFGRS S408Z283	-	22: 5:26.54	-31:33:34.10	2618	13.50±0.135	0.578	0.0
2dFGRS S409Z237	-	22: 6:18.58	-32:10:32.00	2742	13.50±0.099	0.679	0.0
2dFGRS S409Z216	-	22: 7:15.58	-32:12:33.20	2393	13.50±0.071	0.829	0.0
2dFGRS S409Z198	-	22: 7:53.84	-31:56:55.20	2651	13.50±0.135	0.912	0.0
2dFGRS S409Z193	-	22: 8: 6.79	-31:44:57.70	2486	13.50±0.072	0.953	0.0
2MASX J22090574-3147414	-	22: 9: 5.76	-31:47:41.70	2381	12.52±0.189	0.104	2.0
IC 1459							
NGC 7418	6dF J2256361-370148	22:56:36.13	-37: 1:47.80	1417	8.91±0.405	0.250	5.8
IC 5269B	6dF J2256367-361459	22:56:36.72	-36:14:59.09	1638	10.94±0.377	0.142	5.9
NGC 7418A	-	22:56:41.15	-36:46:21.20	2102	13.50±0.497	0.131	6.6
IC 5264	-	22:56:53.04	-36:33:14.99	1940	9.36±0.213	0.032	2.2
NGC 7421	6dF J2256543-372050	22:56:54.33	-37:20:50.70	1801	9.53±0.478	0.394	4.0
IC 1459	6dF J2257106-362744	22:57:10.61	-36:27:44.20	1713	6.93±0.441	0.028	-5.0
2MASX J22571092-3640103	-	22:57:10.92	-36:40:10.40	1945	13.05±0.134	0.071	-3.5
ESO 406- G 031	6dF J2257408-352349	22:57:40.76	-35:23:49.40	1592	13.50±0.162	0.537	1.9
IC 5269	-	22:57:43.66	-36: 1:34.40	1967	9.56±0.366	0.245	-1.6
IC 5270	6dF J2257549-355129	22:57:54.86	-35:51:28.50	1929	9.70±0.396	0.328	5.7
NGC 7714							
SDSS J233631.29-002943.3	-	23:36:31.29	0:29:43.30	2495	13.50±0.100	0.125	99.9
NGC 7716	-	23:36:31.46	0:17:50.30	2571	9.46±0.207	0.010	2.9
SHOC 608	-	23:36:46.84	0:37:24.50	2633	13.50±0.100	0.216	99.9
UGC 12709	-	23:37:24.02	0:23:30.10	2682	13.50±0.129	0.155	8.3

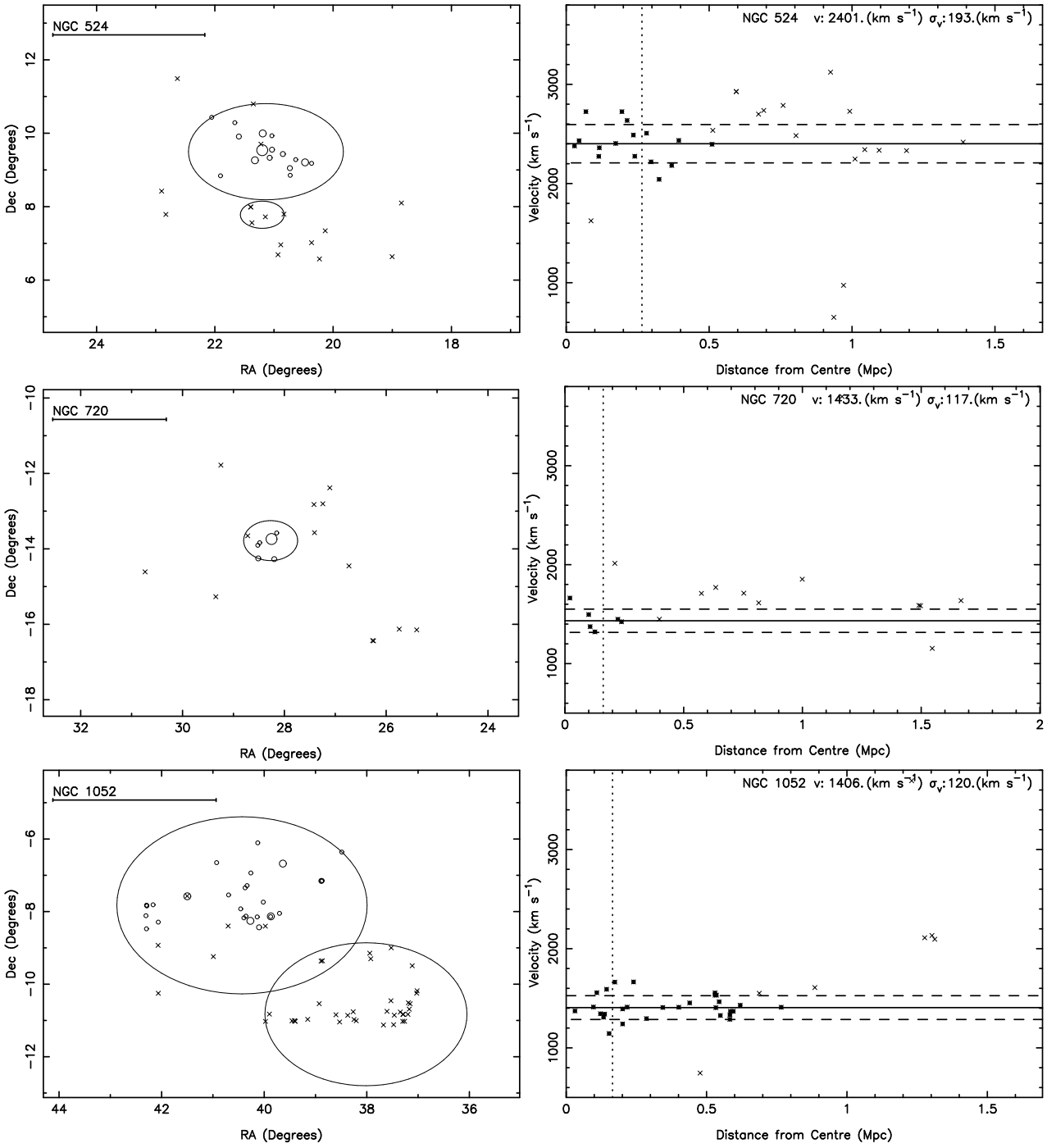

Figure B1. The left-hand panel indicates the spatial distribution of the galaxies in each region. The ellipses mark the maximum extent of all groups determined by FOF. The circles indicate group members defined by FOF, scaled by M_K . The crosses indicate other galaxies in the same field. The line in the top left-hand corner indicates 1 Mpc at the distance of the group being studied. The right-hand panel shows the velocity-distance plots for each group, the centroid defined by FOF. The solid line marks the mean velocity while the dashed lines indicate the velocity dispersion. The vertical dotted line marks the r_{500} radius from Table 3. Solid points mark the group members defined by FOF (shown as open circles in the left-hand panels) and crosses indicate other galaxies in the same region.

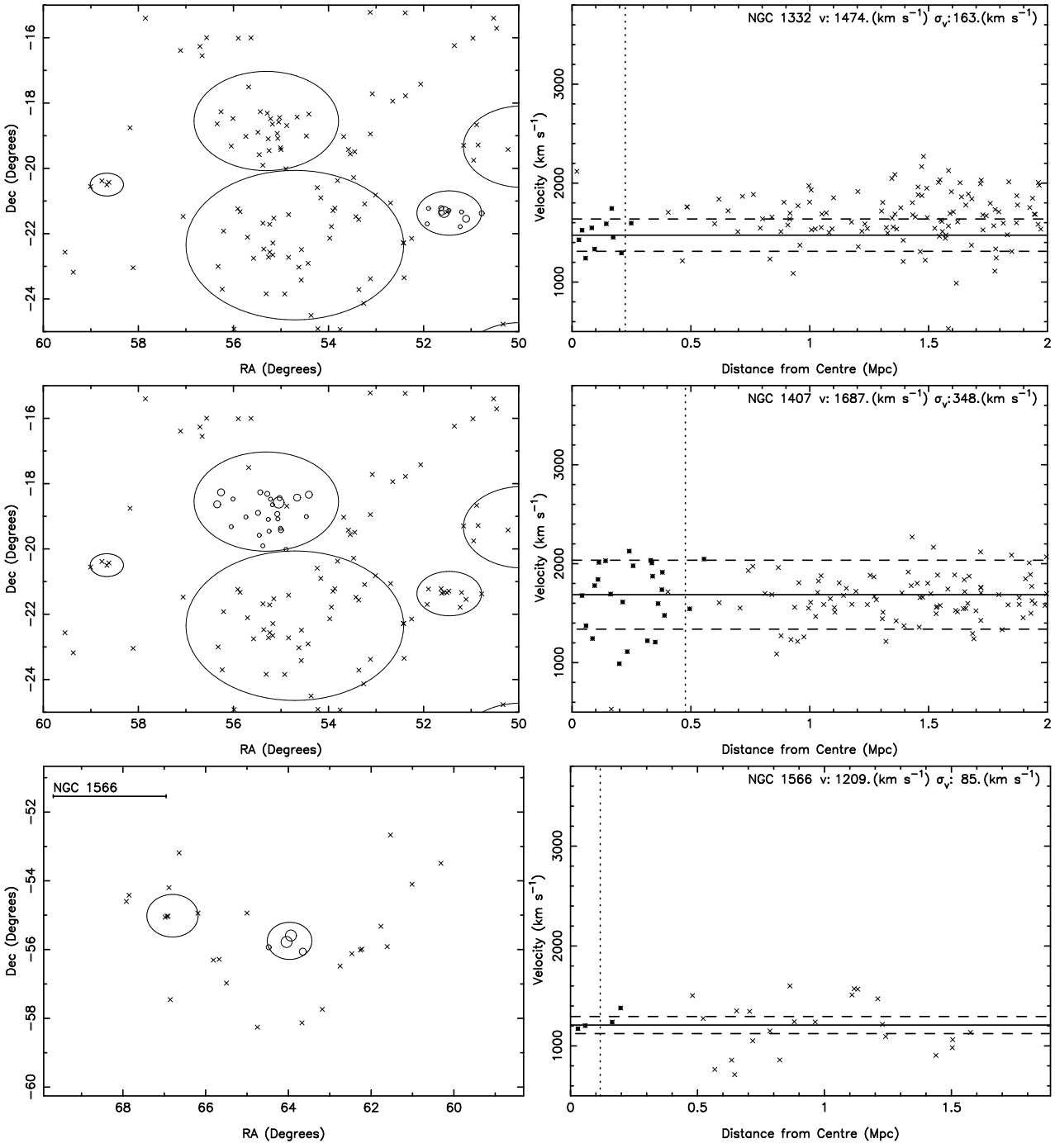

Figure B2. Continued.

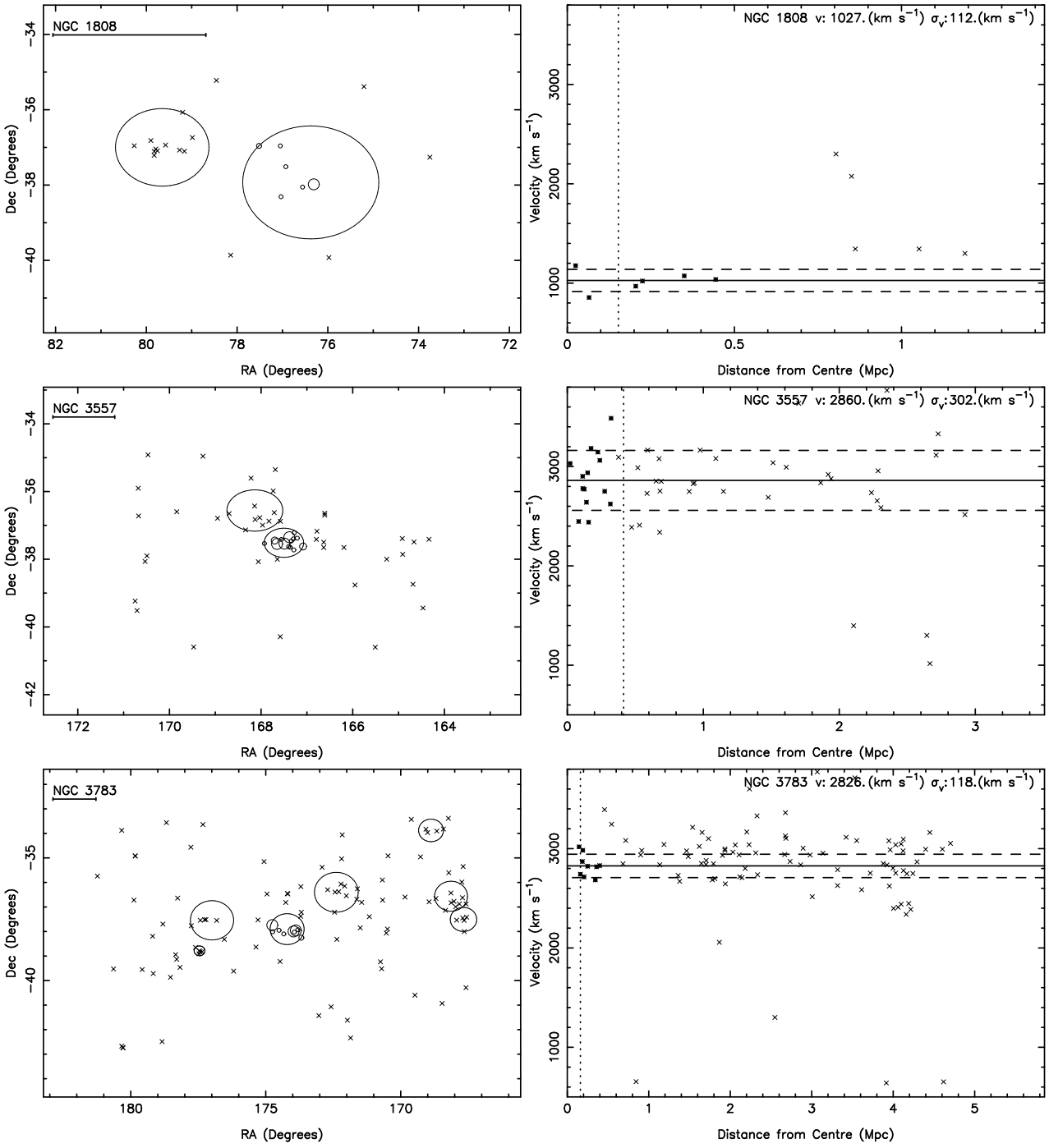

Figure B3. Continued.

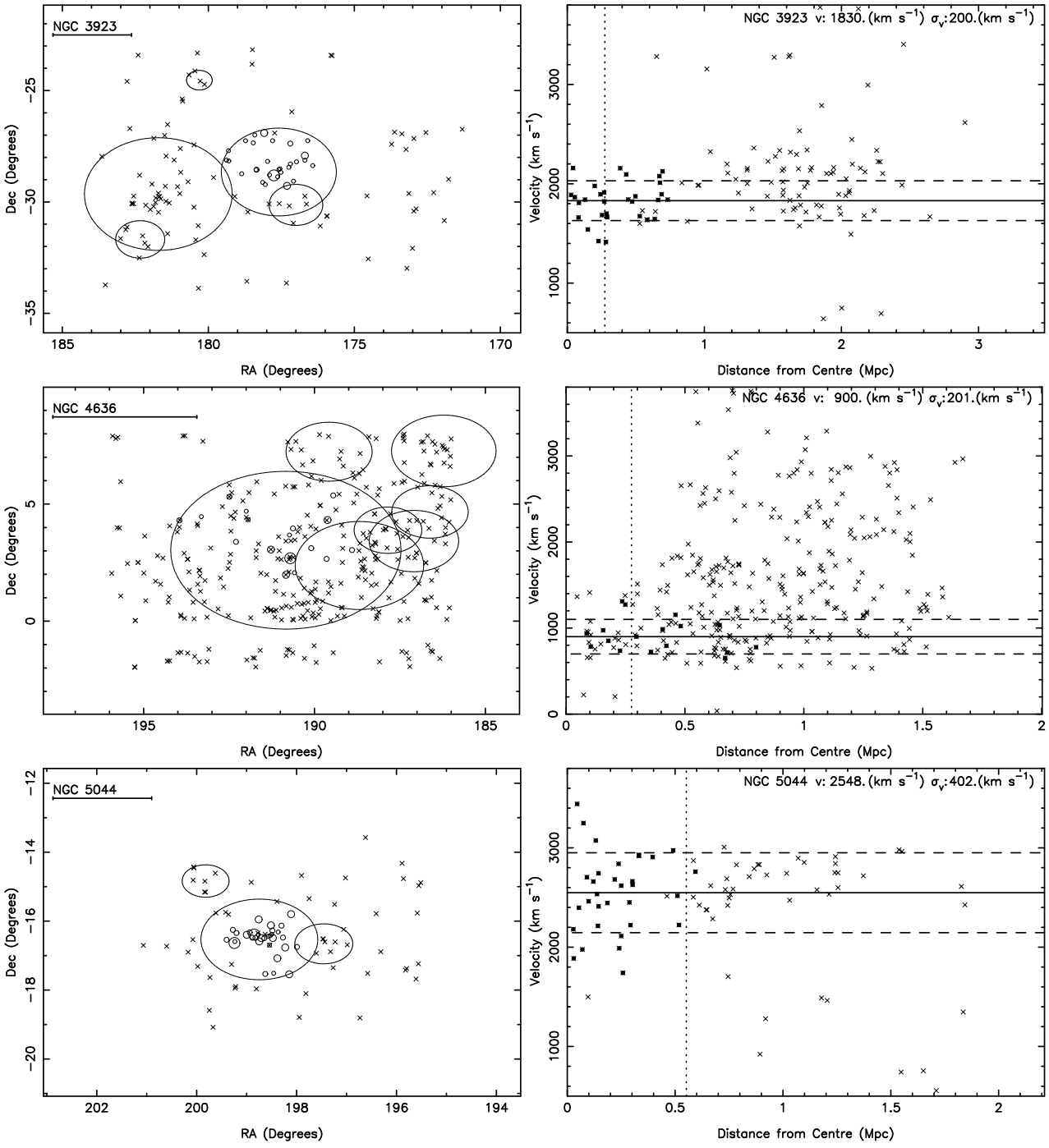

Figure B4. Continued.

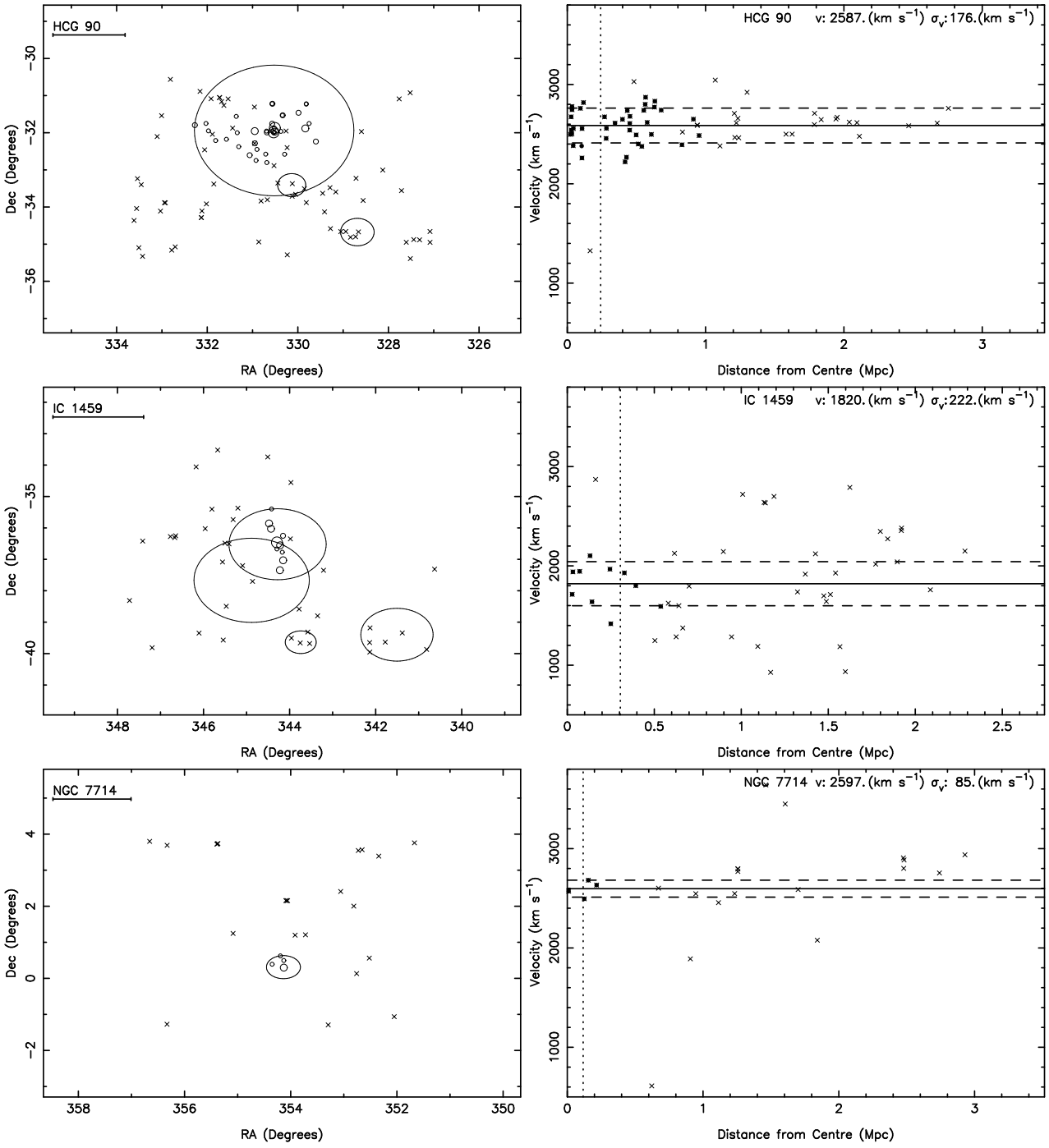

Figure B5. Continued.